Muon-spin relaxation in *Au*Fe and *Cu*Mn spin glasses

Y. J. Uemura
Brookhaven National Laboratory, Upton, New York 11973
and Department of Physics, University of Tokyo, 7-3-1 Hongo, Bunkyo-ku, Tokyo, Japan

T. Yamazaki
Department of Physics, University of Tokyo, 7-3-1 Hongo, Bunkyo-ku, Tokyo, Japan

D. R. Harshman, M. Senba, and E. J. Ansaldo*
TRIUMF, University of British Columbia, Vancouver, British Columbia, Canada
(Received 22 June 1984)

Zero- and longitudinal-field muon-spin relaxation (ZF μSR and LF μSR) measurements have been applied to dilute-alloy spin glasses *Au*Fe(1.0 and 1.4 at %) and *Cu*Mn(1.1, 3, and 5 at. %). A stochastic theory of muon-spin relaxation has been formulated, and an analytic form of zero-field (ZF) muon-spin-relaxation function has been derived to describe the depolarization of muon spins in static, dynamic, and coexisting static and dynamic random local fields from magnetic impurities. The observed experimental results for the muon-spin-relaxation function $G_z(t)$ in all the specimens have been well explained by the model functions based on the present theory. Depolarization of muon spins due to the rapidly fluctuating dynamic local field has been indicated by the "root-exponential" shape of $G_z(t)$ observed above the susceptibility-cusp temperature T_g. The spin correlation time τ_c of Mn (or Fe) moment, deduced from the dynamic depolarization rate of muon spins, shows a rapid change from $\tau_c \sim 10^{-12}$ sec at $T \gtrsim 2T_g$ towards $\tau_c \sim 10^{-9}$ sec at $T \sim T_g$ in all the specimens. Coexistence of static and dynamic random fields at each muon site has been found by ZF and LF μSR below T_g. The average amplitude a_s of static random fields, determined precisely by ZF μSR, attains finite values only below T_g, and increases towards the full amplitude a_0 at $T=0$. a_s/a_0 is proportional to the static polarization of Mn (or Fe) moment, and its temperature dependence has been found to be consistent with a Mössbauer-effect study in *Au*Fe. The squared quantity $(a_s/a_o)^2$ of ZF μSR shows good agreement with the static order parameter $Q(T)$ determined by ac-susceptibility (χ_{ac}) and by neutron-spin-echo (NSE) measurements for cut-off pieces of the same specimen. In view of the fundamental difference of the hyperfine-field—type from the susceptibility-type measurements, this comparison reveals that spin freezing is characterized by a rather homogeneous amplitude of static spin polarization among different spins in spin glasses, i.e., "homogeneous freezing." The combined results of ZF μSR, χ_{ac} and NSE measurements in *Au*Fe and *Cu*Mn spin glasses have demonstrated rapid slowing down of impurity spin fluctuations above T_g, and the appearance of long-time, persisting static spin polarization below T_g.

I. INTRODUCTION

The spin-glass problem has been actively investigated during the past decade.[1-2] After the pioneering work of Cannella and Mydosh in *Au*Fe,[3] many random-spin systems have been found to exhibit a sharp cusp in the ac susceptibility χ_{ac} at the "cusp temperature" T_g. The spatial spin correlation of these systems is basically random at any temperature, without staggered magnetization at any particular wave-vector component, whereas some properties below T_g (e.g., remanent magnetization) depend on the thermal history.[4] These features suggest a new type of spin ordering (or freezing) of such random-spin systems, now called spin glasses. Since the dynamic fluctuations of each magnetic moment play an essential role in spin-glass behavior,[5,2] it is very important to accumulate experimental information on the spin dynamics of spin glasses.

Muon-spin-relaxation (μSR) measurement[6] is a powerful tool for this purpose. This technique was first applied to *Cu*Mn and *Au*Fe spin glasses by Murnick *et al.*[7] They observed the spin precession of μ^+ around the applied transverse magnetic fields, and they found a rapid increase of the muon-spin depolarization rate when T_g was approached from higher temperatures. Similar transverse-field μSR (TF μSR) measurements were also performed later in *Cu*Mn (Ref. 8) and *Ag*Mn (Ref. 9). It was not possible, however, to distinguish the effects of static inhomogeneous random fields from those of fluctuating dynamic fields since the TF μSR experiment corresponds to the "T_2" measurement of magnetic resonance. This difficulty also limited the information obtained from previous linewidth measurements in NMR (Ref. 10) and ESR (Ref. 11) on spin glasses. Furthermore, such experiments with external magnetic fields are not quite suitable for probing spin glasses, in which the sharp "cusp" of susceptibility is substantially rounded by a small external magnetic field.[3]

To overcome these difficulties, we have applied the zero-field μSR (ZF μSR) technique to spin glasses,[12] and have performed a series of measurements on the most typical spin-glass systems, *Cu*Mn and *Au*Fe.[13,14] We have also made measurements on *Cu*Mn in finite longitudinal magnetic fields[15,16] to separate the static and dynamic effects unambiguously. In this paper we provide a comprehensive full description of these studies. We include a stochastic theory of spin relaxation in dilute-alloy spin glasses, and the experimental results on *Cu*Mn(1.1, 3, and 5 at. %) and *Au*Fe(0.94 and 1.4 at. %). The results are compared with neutron-spin-echo (NSE) and ac-susceptibility (χ_{ac}) measurements made on cut-off pieces of the same specimens. In the earlier stage of the present study,[12,13] we assumed simple exponential decay of Mn (or Fe) spin correlation at all the temperatures above and below T_g. With recent high-statistics data, we see in this paper that the static and dynamic random local fields from Mn (or Fe) moments coexist at each muon site below T_g. The amplitude of static random fields, i.e., a quantity proportional to the square root of the Edwards-Anderson order parameter Q,[5] is determined precisely and compared with the results of other techniques. The fundamental difference of hyperfine-field—type experiments (μSR, Mössbauer effect) from susceptibility-type experiments (χ_{ac}, NSE) allows us to investigate the homogeneity of the frozen component among different Mn (or Fe) spins below T_g.

In Sec. II we explain the procedure for the present μSR experiments. In Sec. III we provide a complete description of a stochastic theory of muon-spin relaxation in dilute-alloy spin glasses. Experimental results of the present μSR studies in *Au*Fe and *Cu*Mn are introduced in Sec. IV and are compared with the results of Mössbauer effect, χ_{ac}, and NSE experiments in Sec. V. We discuss some points in detail and summarize the present study in Sec. VI.

II. EXPERIMENTAL PROCEDURE

The zero-field μSR (ZF μSR) and longitudinal-field μSR (LF μSR) methods were established at TRIUMF[17,18] about five years ago. Figure 1 illustrates these techniques. Owing to the parity-nonconservation of weak interaction, muon spins are polarized by nature along the beam direction. We stop the muon beam in a specimen (dotted area of Fig. 1), identify this "stopped-μ" event by the counter M, and start a clock in the data-acquisition system. The decay positron emitted from this μ^+ is recorded by the counter EF (or EB), which produces a logic pulse to stop the clock and thus tells us the residence time t of μ^+ in the specimen. Plotting the positron event rate versus time t, we obtain two sets of muon-lifetime histograms for forward (EF) and backward (EB) counters in ZF and LF μSR. Since positrons are emitted preferentially to the direction of muon spin, the counting rates of EF and EB exhibit asymmetry which reflects the spin polarization of μ^+ at time t, as shown in Fig. 1:

$$N_{EF}(t)=N_F \exp(-t/\tau_\mu)[1+AG_z(t)] ,$$
$$N_{EB}(t)=N_B \exp(-t/\tau_\mu)[1-AG_z(t)] . \quad (1)$$

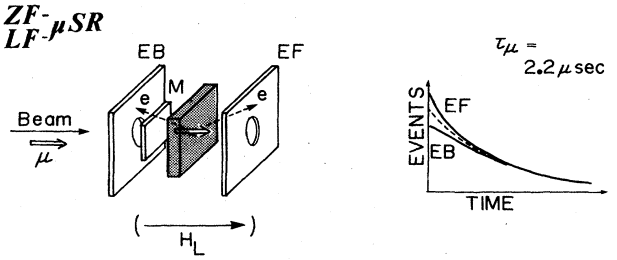

FIG. 1. Schematic view of the counter configuration for zero- and longitudinal-field μSR (ZF and LF μSR) experiments. The polarized-muon beam is stopped in the specimen (dotted area), the "stopped-muon" event is identified by the counter M, and the decay positron is detected by the counter EF or EB. The lifetime histogram of muon decay exhibits asymmetry, reflecting the spin polarization of μ^+ in the specimen.

Here, τ_μ is the positive muon lifetime, 2.2 μsec, A denotes the intrinsic initial muon-decay asymmetry (usually $A=0.2$—0.3), and the muon-spin-relaxation function $G_z(t)$ represents the depolarization of muon spins in the specimen.

When the muon spin is not depolarized, $G_z(t)=1$, and the ratio of N_{EF} and N_{EB} is about 1.2:0.8 after normalization of the solid-angle factors N_F and N_B of the different counters. The ratio becomes 1:1 when muon spin is completely depolarized [$G_z(t)=0$]. In this way, from the asymmetry of N_{EF} and N_{EB}, we can directly observe muon-spin depolarization in ZF μSR even without applying any external magnetic field. The measurements can also be performed by applying a longitudinal external magnetic field H_L parallel to the initial spin direction of μ^+ (LF μSR). The observed time evolution $G_z(t)$ of muon-spin polarization reflects amplitudes, randomness, and fluctuations of local magnetic fields at muon sites in the specimen. The application of ZF and LF μSR to the case of nuclear dipolar systems is described in Ref. 18, and the "T_1" measurements in ferro and antiferromagnetic materials are presented in Refs. 17 and 19.

In the earlier part of the present work, we used a muon beam of average incident momentum $p=140$—180 MeV/c. Even after being slowed down by a polyethylene degrader placed in front of the counter system, some of the muons were energetic enough to traverse the sample. To discriminate such "straight through" muons from the "stopped muons," we placed a counter just behind the specimen and put its anticoincidence into "stopped-muon" logic. This caused an electronics dead time of 20—30 nsec in the observed histogram after $t=0$. Because the data on $G_z(t)$ at $t \lesssim 30$ nsec are very important, especially in relatively concentrated spin glasses, we eliminated this dead time in recent measurements by using the so-called "surface-muon" beam. The surface muons have a very low and discrete incident momentum $p=29$ MeV/c, and 100% of them are stopped within about 200 mg/cm^2 of the specimen.[20] Here we do not need to use the anticoincidence counter, and the observed spectra are free of the dead time. An electrostatic Wien filter, used to separate the surface-muon beam from the contaminating beam particles,[20] has been helpful in keeping the back-

TABLE I. Specimens and related references.

Specimen	Concentration (at. %)	T_g (K)	References
*Au*Fe	1.0	9.1	χ_{ac} (39)
	1.4	12.8	
*Cu*Mn	1.1	10.8	
	3	20.0	neutron (48)
	5	27.4	NSE (43)
			χ_{ac} (45)

ground very low. The high-intensity surface-muon beam at TRIUMF has thus enabled us to obtain high-statistics data on $G_z(t)$ for *Cu*Mn specimens in a wide time range, 4 nsec $\lesssim t \lesssim$ 10 μsec.

In order to make a reliable comparison with other experimental techniques, we used cut-off pieces from the same ingot specimens examined in ac-susceptibility, neutron-spin-echo, and neutron time-of-flight measurements. In Table I we give the concentration c, cusp temperature T_g, and related references for each specimen. At the beginning of the present study we noticed that the μSR results depended on the heat treatment of the sample preparation. *Cu*Mn specimens prepared by quenching from high temperatures ($\sim$850 °C) exhibited much sharper temperature dependence of $G_z(t)$ around T_g than did specimens made by slow cooling.[12] A similar tendency for the sharpness of the susceptibility cusp was reported by Mulder *et al.*[21] Electron-microprobe analysis showed that this is due to semimacroscopic inhomogeneity of impurity concentration developed in slowly cooled samples.[12] We therefore report here the results on *Cu*Mn specimens prepared by quenching from $T\sim$1100 K and *Au*Fe specimens prepared by rapid cooling after arc melting. The *Au*Fe and *Cu*Mn(1.1 at. %) specimens were checked by chemical analysis and electron microprobe (homogeneous impurity concentration within $\pm$5% of nominal concentration among several different spots of 10 μm diameter), and the sharpness of the observed susceptibility cusp also confirmed that these specimens were "good" spin glasses.

III. STOCHASTIC THEORY OF MUON-SPIN RELAXATION IN SPIN GLASSES

A. Distribution of local fields and static relaxation functions

The following features (A)–(C) are helpful in characterizing local fields at a muon site.

(A) No muon diffusion. Studies of nuclear dipolar fields on μ^+ (Ref. 22) have shown that a positive muon occupies an octahedral interstitial site in pure Cu and remains stationary up to $t\sim$10 μsec without diffusion over the temperature range $3<T<70$ K. From the characteristic shape of $G_z(t)$ observed at $T\gtrsim 1.5T_g$, we confirmed that this is the case also for μ^+ in *Cu*Mn spin glasses. Although no direct information is available for *Au*Fe because of the lack of nuclear dipolar fields, we assume that the situation is the same in such systems of other fcc noble metals.

(B) Random selection of interstitial sites. We assume that all the octahedral interstitial sites have an equal probability of being a muon site, regardless of the position of neighboring Mn (or Fe) atoms. Strong support for this assumption will be provided by the observed amplitudes of average random local fields on μ^+.

(C) Dominant atomic dipolar fields. Because of weak coupling between conduction electrons and muon spins [the Knight shift, $\sim$50 ppm, of μ^+ in pure Cu (Ref. 23) is more than 40 times smaller than the shift, $\sim$2300 ppm, for the host Cu nuclei (Ref. 24)], the average Ruderman-Kittel-Kasuya-Yosida (RKKY) field at a muon site in *Cu*Mn(1 at. %) is only about 10 G.[25] The atomic dipolar field is around 100 G and the nuclear dipolar field from Cu nuclei is around 4 G.

Thus the random field at a muon site is mainly due to the atomic dipolar field from surrounding Mn (or Fe) moments, and the dynamic modulation is caused only by the fluctuation of these moments. In such a random dilute spin system, the local field due to the $(1/r^3)$-type interaction has a Lorentzian distribution[26,27] for the dilute limit (effectively for concentrations c less than 3–5 at. %). Therefore, we employ the following distribution:

$$P^L(H_i)=\frac{\gamma_\mu}{\pi}\frac{a}{a^2+\gamma_\mu^2 H_i^2},\quad i=x,y,z$$
$$P^L(|H|)=\frac{\gamma_\mu^3}{\pi^2}\frac{a}{(a^2+\gamma_\mu^2|H|^2)^2}4\pi|H|^2, \tag{2}$$

with a half-width at half maximum (HWHM) a/γ_μ ($\gamma_\mu=2\pi\times 1.35\times 10^4$ sec^{-1} Oe^{-1} is the gyromagnetic ratio of the muon spin) to describe the random local fields at muon sites. The superscript L stands for Lorentzian here.

When the random fields are static, one simply calculates the muon-spin precession around $\vec{H}$, finds its projection to the beam direction (z axis), and averages over $P^L(H)$ to obtain the muon-spin-relaxation function $G_z(t)$. This has been done by Kubo,[28] who derived

$$g_z^L(t)=\tfrac{1}{3}+\tfrac{2}{3}(1-at)\exp(-at) \tag{3}$$

for the case of zero external field. This function is shown in Figs. 2 ($\omega_L/a=0$ line) and 4 (dotted line). The persisting $\frac{1}{3}$ component represents muons stopped where the local field is rather parallel to the initial spin direction z, while the inhomogeneity of H_x and H_y causes the damped oscillation of the $\frac{2}{3}$ component. In a longitudinal field $H_L=\omega_L/\gamma_\mu$ applied parallel to z, a similar calculation yields

$$g_z^L(t,H_L)=1-\frac{a}{\omega_L}j_1(\omega_L t)\exp(-at)-\left[\frac{a}{\omega_L}\right]^2[j_0(\omega_L t)\exp(-at)-1]-\left[1+\left[\frac{a}{\omega_L}\right]^2\right]a\int_0^t j_0(\omega_L\tau)\exp(-a\tau)d\tau, \tag{4}$$

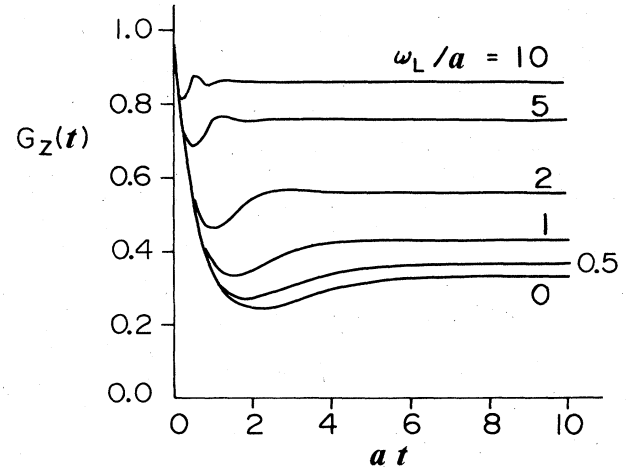

FIG. 2. Muon-spin-relaxation function of Eq. (4) calculated for Lorentzian distribution of static random local fields in a longitudinal external magnetic field H_L ($\omega_L=\gamma_\mu H_L$). The line shape for $\omega_L/a=0$ corresponds to the zero-field function of Eq. (3), and the finite longitudinal field works as a "decoupling" field to increase the persistent component from $\frac{1}{3}$ in zero field to larger values.

where j_0 and j_1 denote spherical Bessel functions. As shown in Fig. 2, the longitudinal field H_L works as a "holding (or decoupling)" field to increase the persisting component and to eliminate the effect of static random fields H_x and H_y. The average amplitude a of random fields can be observed via the damping rate of the $\frac{2}{3}$ component in ZF μSR and also via the field dependence of the persisting component in LF μSR.

B. Relaxation functions in fluctuating random fields

When Mn (or Fe) moments fluctuate, the local field at each muon site is modulated. The variable range of the field modulation is, however, different from site to site, depending on the configuration of surrounding impurities, as illustrated in Fig. 3. Following the treatment of Uemura,[12] let us here approximate this dynamic variable range at each site by a Gaussian distribution having width Δ/γ_μ (henceforth, superscript G stands for Gaussian):

$$P^G(H_i)=\frac{\gamma_\mu}{\sqrt{2\pi}\Delta}\exp\left[-\frac{\gamma_\mu^2 H_i^2}{2\Delta^2}\right],\quad i=x,y,z\ . \tag{5}$$

Assuming Markovian modulation of the field H with a rate ν,

$$\langle H(t)H(0)\rangle/\langle[H(0)]^2\rangle=\exp(-\nu t)\ , \tag{6}$$

within the variable range $P^G(H,\Delta)$, the zero-field muon-spin-relaxation function at each site can be calculated via the strong-collision approximation[12,18] as

$$G_z^G(t,\Delta,\nu)=\exp(-\nu t)\left[g_z(t)+\nu\int_0^t g_z(t_1)g_z(t-t_1)dt_1+\nu^2\int_0^t\int_0^{t_2} g_z(t_1)g_z(t_2-t_1)dt_1\,dt_2+\cdots\right], \tag{7}$$

where $g_z(t)$ denotes the static relaxation function. For $P^G(H)$, the static function becomes the so-called Kubo-Toyabe[29] function:

$$g_z^G(t,\Delta)=\tfrac{1}{3}+\tfrac{2}{3}(1-\Delta^2t^2)\exp(-\tfrac{1}{2}\Delta^2t^2)\ . \tag{8}$$

The numerical calculation of $G_z^G(t,\Delta,\nu)$ using Eqs. (7) and (8) is given in Ref. 18.

The probability $\rho(\Delta)$ of finding a muon site with Δ can be calculated as

$$\rho(\Delta)=\sqrt{2/\pi}\frac{a}{\Delta^2}\exp\left[-\frac{a^2}{2\Delta^2}\right], \tag{9}$$

$$P^L(H_i)=\int_0^\infty P^G(H_i)\rho(\Delta)d\Delta\ , \tag{10}$$

so that the total field distribution should be Lorentzian. Then, averaging the signals from different muon sites, Uemura[12] gave the dynamic muon-spin-relaxation function for the entire system as

$$G_z^{SG}(t,a,\nu)=\int_0^\infty G_z^G(t,\Delta,\nu)\rho(\Delta)d\Delta\ . \tag{11}$$

This function is shown in Fig. 4. Note the importance of the order of the two operations, i.e., static → dynamic [Eq. (7)] and spatial averaging [Eq. (11)]. If we reverse the order of these operations and substitute Eq. (3) for

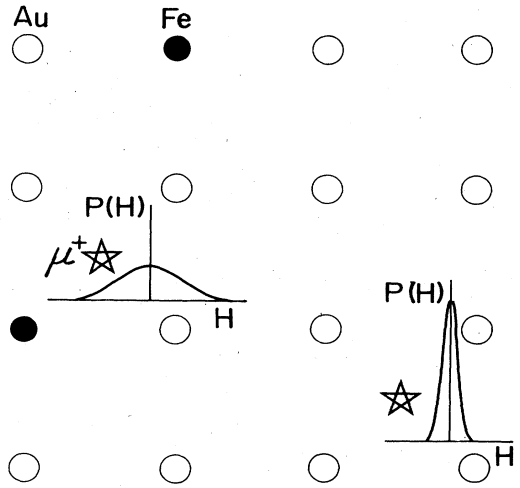

FIG. 3. Schematic view of different variable ranges of random local fields at different muon sites in dilute-alloy spin glasses. When Fe (or Mn) moments fluctuate, the local field at muon sites closer to the magnetic ions will be modulated in a wider range.

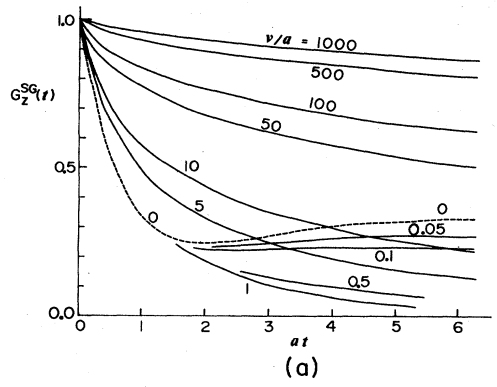

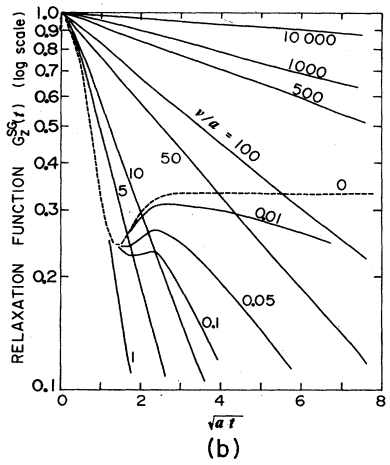

FIG. 4. Zero-field muon-spin-relaxation function of Eq. (11) calculated in a fluctuating dynamic random local field that follows the simple Markovian modulation of Eq. (6) with a rate ν. The line shape for the static limit $\nu \to 0$ (dashed lines) becomes Eq. (3), while the "root-exponential" decay of Eq. (13) is obtained for $\nu/a \gg 1$.

$g_z(t)$ in Eq. (7), we obtain a totally different relaxation function. This is a good example for demonstrating that spatial averaging should always be done at the final point of any calculation in random systems.

For the static case $\nu \to 0$, $G_z^{SG}(t,a,\nu)$ becomes $g_z^L(t)$ of Eq. (3), as shown by the dotted line in Fig. 4. The slow modulation $\nu/a \lesssim 1$ of random fields causes decay of the persisting $\frac{1}{3}$ component as $G_z(t) \sim \frac{1}{3}\exp(-2\nu t/3)$, while the initial damping rate of the $\frac{2}{3}$ component is kept unchanged up to $\nu/a \sim 1$. Faster modulation, $\nu/a > 2$, effectively averages the randomness of the local fields and reduces the initial decay rate. This corresponds to the so-called "narrowing effect" in magnetic resonance experiments. For fast modulation, $\nu/a \gtrsim 20$, where the function $G_z^G(t,\Delta,\nu)$ at each site becomes

$$G_z^G(t,\Delta,\nu)=\exp(-2\Delta^2 t/\nu)\ , \tag{12}$$

spatial averaging with Eq. (11) yields an analytic form of the muon-spin-relaxation function,

$$G_z(t)=\exp[-(4a^2 t/\nu)^{1/2}]\ , \tag{13}$$

which exhibits "root-exponential" shape. In Fig. 4(b) the numerical result of $G_z^{SG}(t)$ is plotted on a logarithmic scale versus $\sqrt{t}$. The straight lines for $\nu/a \gtrsim 5$ indicate that the relaxation function shows the "root-exponential" decay in the case of rapidly fluctuating random fields. This type of relaxation was observed in early NMR studies[30] of a dilute magnetic system. Fiory[31] made a computer-simulation study of muon-spin relaxation in dilute-alloy spin glasses and obtained results consistent with Eq. (13).

When the Mn (or Fe) moment S is fluctuating randomly following Markovian modulation without any spatial correlation, the time correlation function for the local field H becomes the same as that for the spin S. Therefore we can deduce the rate ν of Mn (or Fe) spin fluctuations by comparing the observed data with the relaxation function $G_z^{SG}(t,a,\nu)$. The characteristic shape of the static function with the $\frac{1}{3}$ tail is helpful in distinguishing the relaxation due to static random fields in ZF μSR. We can also calculate the relaxation functions for finite longitudinal external field $H_L=\omega_L/\gamma_\mu$ in a similar way using Eq. (11). Here, $G_z^G(t,\Delta,\nu)$ for fast modulation becomes

$$G_z^G(t,\Delta,\nu,H_L)=\exp\left[-\frac{2\Delta^2\nu}{\nu^2+\omega_L^2}t\right]\ , \tag{14}$$

which indicates that the μSR spectra do not depend on the longitudinal field H_L when random fields are fluctuating with $\nu \gg \omega_L$. This shows a clear contrast with the substantial field dependence for the static case (Fig. 2), and thus provides another way of discriminating between the static and dynamic effects of random fields in LF μSR.

C. Relaxation functions in coexisting static and dynamic random fields

Below the ordering temperature, in usual ferromagnetic or antiferromagnetic systems, the fluctuation of magnetic moments is not described by a simple exponential autocorrelation function since each spin develops an average static polarization, i.e., staggered magnetization. Even in spin glasses, without long-range spatial ordering of any Fourier component of impurity moments, such a polarization may be realized as a finite probability of each spin being oriented towards its "preferred direction" during the fluctuation. This picture can be described by a nonvanishing part Q of the autocorrelation function of impurity spins,

$$[\langle S(t)S(0)\rangle/\langle[S(0)]^2\rangle]_{av}=(1-Q)\exp(-\nu t)+Q\ , \tag{15}$$

where $\langle\ \rangle$ denotes the thermal average for one impurity moment, and $[\ ]_{av}$ represents the spatial average over different spins. Such an "ordering in time" was suggested by Edwards and Anderson[5] based on the replica theory, and Q is called an order parameter.

The simplest way to simulate Eq. (15) is to assume each spin to be a vector sum of a static component $\sqrt{Q}S$ and a dynamic component $\sqrt{1-Q}S$ fluctuating randomly with

a rate ν. The local field H at a muon site is due to several neighboring Mn (or Fe) moments as $H=\sum_i A_i S_i$, where A_i represents magnetic dipolar interaction from the ith spin S_i. When there is no correlation between different neighboring spins, the cross term $\langle S_i(0)S_j(t)\rangle$ vanishes. Then the autocorrelation function $\langle H(t)H(0)\rangle/\langle[H(0)]^2\rangle$ for H has the same form as Eq. (15), and the local field at a muon site is described by the same vector sum as for the spin S. When the fluctuation of the dynamic component is appreciably fast ($\nu/a \gg 1$), the spin-relaxation function at each muon site $G_z^{\rm G}(t,\Delta,\nu,Q)$ is given by a product of static and dynamic relaxation functions as

$$\Delta_s=\sqrt{Q}\,\Delta,\quad \Delta_d=\sqrt{1-Q}\,\Delta\ ,$$
$$G_z^{\rm G}(t,\Delta,\nu,Q)=g_z^{\rm G}(t,\Delta_s)G_z^{\rm G}(t,\Delta_d,\nu)\ , \tag{16}$$

where Δ_s and Δ_d correspond to widths of Gaussian local fields representing the static and dynamic component at each muon site, and

$$g_z^{\rm G}(t,\Delta_s)=\tfrac{1}{3}+\tfrac{2}{3}(1-\Delta_s^2t^2)\exp(-\tfrac{1}{2}\Delta_s^2t^2)$$

[as given by Eq. (8) with $\Delta=\Delta_s$] and

$$G_z^{\rm G}(t,\Delta_d,\nu)=\exp(-2\Delta_d^2t/\nu)$$

[as given by Eq. (12) with $\Delta=\Delta_d$]. Then, by taking the spatial average over $\rho(\Delta)$ of Eq. (9) as in Eq. (11), we obtain a model function for the entire system which includes the effect of Q.

For the case of zero field, this integration can be performed analytically, and we obtain

$$G_z(t)=\tfrac{1}{3}\exp[-(4a_d^2t/\nu)^{1/2}]+\frac{2}{3}\left[1-\frac{a_s^2t^2}{(4a_d^2t/\nu+a_s^2t^2)^{1/2}}\right]\exp[-(4a_d^2t/\nu+a_s^2t^2)^{1/2}]\ ,$$
$$a_s=\sqrt{Q}\,a,\quad a_d=\sqrt{1-Q}\,a \tag{17}$$

for the muon-spin-relaxation function in the entire system. Figure 5 shows an example of this function at $\nu/a=100$ for various values of Q. In the static limit of $Q\to 1$ and $a_s\to a$, this function becomes $g_z^L(t)$ of Eq. (3), whereas the "root-exponential" shape of Eq. (13) is obtained for the dynamic limit $Q\to 0$, $a_d\to a$, and $\nu/a\gg 1$. As shown in Fig. 5, the line shape of Eq. (17) in coexisting static and dynamic random fields can be characterized by the following features. (1) Quick initial decay of $G_z(t)$; the decay rate increases gradually with increasing static amplitude $a_s/a=\sqrt{Q}$. (2) Slow decay of the "tail"; the $\frac{1}{3}$ "tail" of $G_z(t)$ shows up as a static effect, and the dynamic component of random fields causes its slow damping. The difference of $G_z(t)$ of Eq. (17) from the simpler model function $G_z^{\rm SG}(t)$ [Eq. (11)] in the preceding section can be found when we compare Figs. 4(b) and 5(b). In Fig. 4(b) the "tail" of $G_z^{\rm SG}(t)$ is expected only with the quickest initial decay (see $\nu/a<1$), and the "tail" completely disappears even when the initial decay rate is reduced slightly by the narrowing effect (see, e.g., $\nu/a=5$). In contrast, the "tail" of the relaxation function can be found with various rates of initial decay in Fig. 5(b). Uemura[32] made a calculation of $G_z(t)$ for finite Q based on a slightly different model, and obtained results consistent with those in Fig. 5. Calculations for finite longitudinal fields can be performed in a similar way to the case of zero field.

The so-called "cluster model" represents another view of spin-glass freezing.[4] Here one assumes that the system is divided into clusters (or domains), each having its own correlation time $\tau_{\rm cl}$ which differs from cluster to cluster. If each cluster contains more than about 100 impurity spins, the dominant local field at most muon sites would originate from the impurities within one cluster. In that case the spin-relaxation function of muons in the cluster is given by $G_z^{\rm SG}(t,a,\nu_{\rm cl})$ with the modulation rate $\nu_{\rm cl}=1/\tau_{\rm cl}$

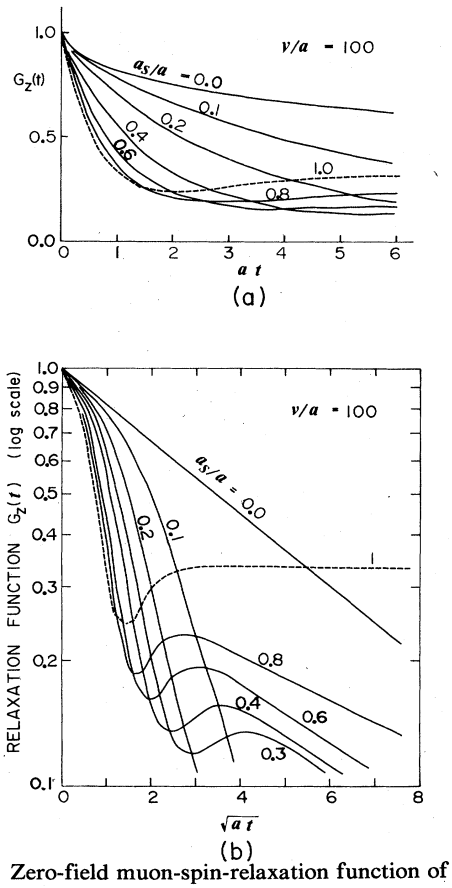

FIG. 5. Zero-field muon-spin-relaxation function of Eq. (17), calculated for coexisting static and dynamic random local fields at each muon site, with dynamic modulation rate $\nu/a=100$ and various static amplitudes a_s. The increasing static amplitude of random fields causes increasingly quick initial decay of $G_z(t)$ followed by the slowly damping "tail."

of the cluster. If the system is an assembly of such clusters, we have only to integrate $G_z^{SG}(\nu_{cl})$ over a probability distribution $P(\nu_{cl})$ of ν_{cl} (proportional to the number of muon sites with ν_{cl}) to calculate the muon-spin-relaxation function expected in the entire system. It is, however, difficult to calculate $G_z(t)$ when the correlation time $\tau_c = 1/\nu$ of impurity moments has a distribution in a more "microscopic" way. Suppose a muon site is surrounded by three Mn moments fluctuating with $\nu/a = 100$, 1, and 0.01. The field from spins of $\nu/a = 1$ and 0.01 causes quick initial damping of $G_z(t)$ to $\frac{1}{3}$, whereas the following damping of $G_z(t)$ at the muon site is due mainly to the $\nu/a = 1$ spin. Here the time evolution of the local field at a muon site becomes so complicated that $G_z(t)$ cannot be calculated either by a simple average or by a product of different relaxation functions.

D. Amplitude of random fields

In spin glasses the exchange field at a Mn (or Fe) spin S from neighboring moments causes fast precession of S and defines the randomly oriented quantization axis ψ of each spin S at low temperatures. This precession is much faster than the muon spin precession around its local field H, and averages out the component of S perpendicular to ψ. Therefore, only the component of S parallel to ψ contributes to the local field H at muon sites. Then the Gaussian width Δ^2 of the atomic dipolar field at a muon site from surrounding moments becomes

$$\Delta^2 = \tfrac{2}{3} \sum_m P(m) m^2 \hbar^2 \gamma_\mu^2 \gamma_e^2 \sum_k r_k^{-6} , \tag{18}$$

where m denotes the magnetic quantum number of the spin S referred to ψ, $P(m)$ gives its occupation probability, and the summation of k runs over the impurity atoms. The finite order parameter Q is embodied when $P(m)$ tends to have a preference for the ground state $m = S$. At zero temperature, $P(m = S) = 1$ and all the other states are empty. Then we have

$$\Delta^2 = \tfrac{2}{3} S^2 \hbar^2 \gamma_\mu^2 \gamma_e^2 \sum_k r_k^{-6} \tag{19}$$

for the lattice sum.

To calculate the static width a of random fields, a convenient equation can be derived by using $\rho(\Delta)$ of Eq. (9). Let us define Δ_{max}^2 as the hypothetical dipolar width expected when all the lattice points are filled up with impurity spins ($c = 100$ at. %). Since Δ^2 is an additive quantity for each impurity spin, the averaged dipolar field on μ^+ in a dilute alloy can be expressed as

$$\langle \Delta^2 \rangle = c \Delta_{max}^2 , \tag{20}$$

$$\langle \Delta^2 \rangle = \int_0^{\Delta_{max}} \Delta^2 \rho(\Delta) d\Delta , \tag{21}$$

where c is the impurity concentration. The right-hand side of Eq. (21) becomes

$$\langle \Delta^2 \rangle = \sqrt{2/\pi} a \Delta_{max} \exp\left[-\frac{a^2}{2\Delta_{max}^2} \right] - \sqrt{4/\pi} a^2 \operatorname{erfc}\left[\frac{a}{\sqrt{2}\Delta_{max}} \right] . \tag{22}$$

In the dilute limit $\Delta_{max} \gg a$, the second term of this equation can be neglected compared to the first term, and we obtain a quite simple relation for the random fields in spin glasses from Eqs. (20) and (22) as

$$a = \sqrt{\pi/2} c \Delta_{max} . \tag{23}$$

This treatment can be called a "sum rule," which automatically gives the full width a from the lattice sum and the impurity concentration c.

By using the effective moment $2\sqrt{S(S+1)} = 5.0$ of a Mn spin in *Cu*Mn,[21] we obtain $\Delta_{max} = 1140\ \mu\text{sec}^{-1}$ with Eq. (19) at an octahedral muon site in *Cu*Mn. Consequently, the width a for *Cu*Mn (1 at. %) at $T = 0$ is given by Eq. (23) as $a \sim 14.3\ \mu\text{sec}^{-1}$. This number should be slightly decreased in actual systems since the nuclear dipolar field at a muon site observed in pure Cu by μSR (Ref. 22) was about 10% smaller than that obtained by a similar theoretical calculation of dipolar broadening. It is shown in the next section that the experimental values of a agree reasonably well with the above calculation. As seen in Eqs. (19) and (23), the width a_s of a static field is proportional to the spin S of impurity moments at $T = 0$, and to the static polarization $\sqrt{Q}S$ (i.e., the so-called shuttered magnetization) at finite temperatures. The linear proportionality of a to the concentration c is a characteristic feature of the $1/r^3$ interaction in dilute systems. When we double the concentration, the effective length scale changes by $2^{-1/3}$, making the field H twice as large, while the system maintains "self-similarity" as long as the impurities are dilute. Because of this feature, each spin S makes a linear contribution to the width a. Therefore a_s is proportional to the linear average of static polarization $\sqrt{Q}S$ when Q is different from one spin to another. This point was also noted in the computer simulation of Walstead and Walker.[27]

IV. EXPERIMENTAL RESULTS

In the experiments each specimen (about 2.5 cm in diameter and 2—8 mm thick) was placed in a gas-flow cryostat which stabilized the temperature within ± 0.1 K. We used the high-momentum ($p \sim 140$ MeV/c) muons from the M-9 channel of TRIUMF in ZF μSR of *Au*Fe and LF μSR of *Cu*Mn. For ZF μSR in *Cu*Mn specimens, the surface-muon beam from the M-20 channel of TRIUMF was used with the spectrometer EAGLE (Ref. 33). Here the magnetic field was minimized by a set of compensation coils to be less than about 50 mG. The intrinsic muon-decay asymmetry A was about 0.2 for the high-momentum muons and about 0.3 for the surface muons. In *Cu*Mn, the solid-angle factor N_F/N_B of forward and backward counters was calibrated by fitting the spectra observed at $T \sim 3T_g$. At these high temperatures, $G_z(t)$ exhibited the Kubo-Toyabe function of Eq. (8) for nuclear dipolar fields from Cu nuclei. This function damps towards $G_z(t) \sim 0$ at $t \sim 5\ \mu$sec, where the solid-angle factor can be determined unambiguously. For the case of *Au*Fe, we made a muon-spin-precession measurement in a transverse external field at $T \sim 3T_g$ to check the solid-angle factor.

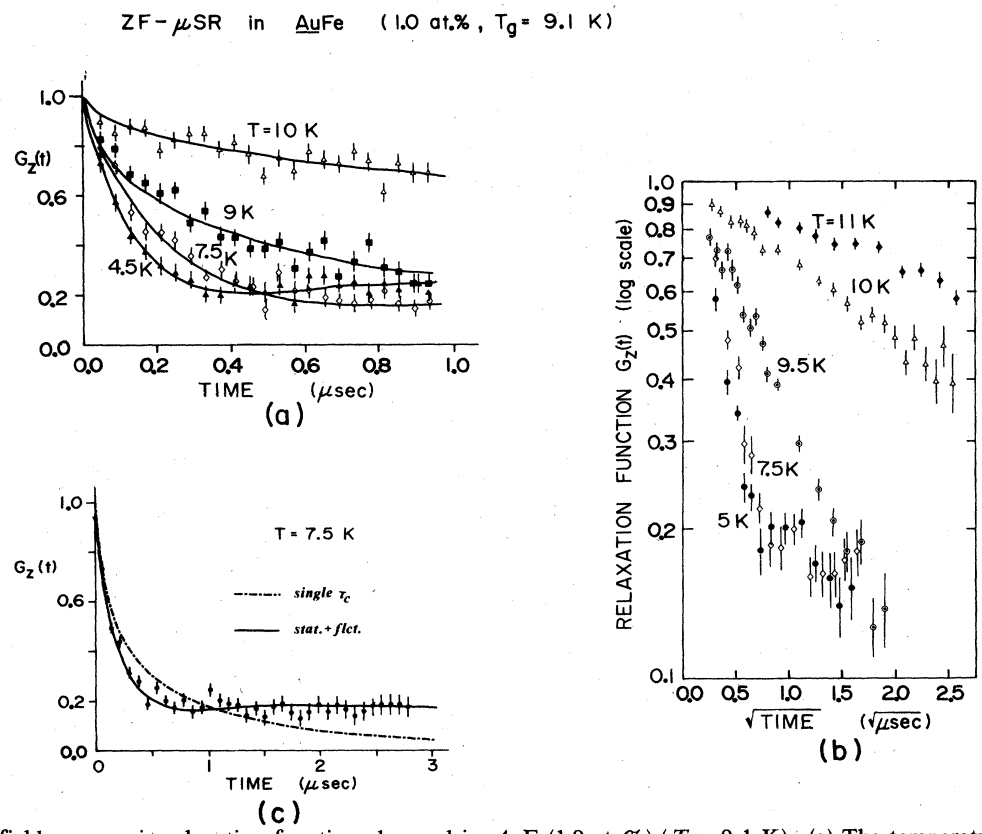

FIG. 6. Zero-field muon-spin-relaxation function observed in *Au*Fe(1.0 at. %) ($T_g=9.1$ K). (a) The temperature dependence of line shapes. (b) Decay of $G_z(t)$ showing "root-exponential" time dependence above T_g, and the temperature-dependent quick initial decay with a "tail" below T_g. (c) Model function of Eq. (17) [or Eq. (24)] for the coexisting static and dynamic random fields, providing a better fit to the data below T_g than the function of Fig. 4, assuming simple exponential time correlation of Fe spins without static polarization. The solid lines in (a) and (c) represent the best-fit curves for Eq. (24).

A. Relaxation functions observed in zero field

Since the nuclear moment of Au is very small and has no effect on the time range of μSR measurements, positive muons in *Au*Fe will directly exhibit the shape of relaxation functions described in the preceding section. Figure 6(a) shows the results for $G_z(t)$ measured by ZF μSR in *Au*Fe(1.0 at. %) ($T_g=9.1$ K). Upon cooling from $T\sim 1.5T_g$ through T_g, the depolarization rate increased rapidly. In Fig. 6(b) we plot $G_z(t)$ on a logarithmic scale versus $\sqrt{t}$ in order to demonstrate that the spin polarization of μ^+ above T_g actually decays with the "root-exponential" time dependence of Eq. (13). Here the data follow the straight lines that correspond to the relaxation

$$G_z(t)=\exp[-(\lambda_d t)^{1/2}] .$$

The relaxation rate λ_d increases as the temperature decreases towards T_g.

Below T_g, the initial damping rate of $G_z(t)$ increases gradually with decreasing temperature as in Fig. 6(a), and this quick damping of $G_z(t)$ to 0.2—0.3 is followed by a slowly damping "tail" as shown in Figs. 6(a)—6(c). These are the characteristic features of the relaxation function of Eq. (17), i.e.,

$$G_z(t)=\tfrac{1}{3}\exp[-(\lambda_d t)^{1/2}]+\frac{2}{3}\left[1-\frac{a_s^2t^2}{(\lambda_d t+a_s^2t^2)^{1/2}}\right]\exp[-(\lambda_d t+a_s^2t^2)^{1/2}] , \tag{24}$$

expected for μ^+ in coexisting static ($\nu/a\ll 1$) and dynamic ($\nu/a\gg 1$) random local fields, which follows the time correlation of Eq. (15). $G_z(t)$, for a series of temperatures below T_g, can be well represented by this line shape, with increasing static amplitude a_s for decreasing temperatures, as shown by the solid lines of Figs. 6(a) and 6(c). The simpler model function of Eq. (11) (Fig. 4), calculated for a single exponential time correlation of H without order parameter Q, is not adequate below T_g. As shown in Fig. 6(c), when we fix the width a of random fields as the number obtained at lower temperatures ($T\sim 0.5T_g$), it is not possible to obtain a good fit to the observed data at $T\sim 0.8T_g$.

In zero-field μSR of *Cu*Mn, nuclear dipolar fields H_{Cu}

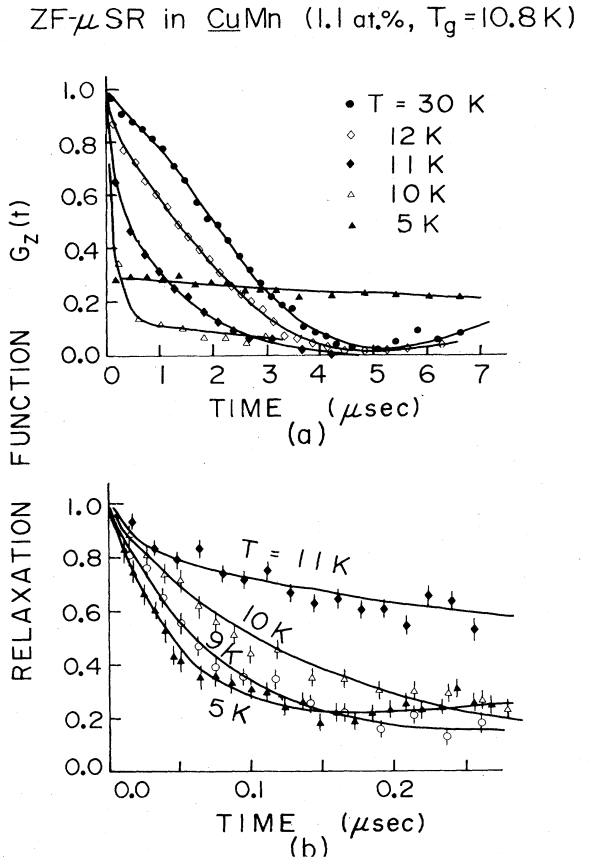

FIG. 7. Zero-field muon-spin-relaxation function observed in *Cu*Mn(1.1 at. %) ($T_g = 10.8$ K). (a) The Kubo-Toyabe function for nuclear dipolar fields from Cu is observed at $T \gg T_g$, and the slowing-down of Mn moments causes the rapid depolarization of muon spins when the temperature is lowered. (b) The rate of quick initial damping of $G_z(t)$ gradually increases with decreasing temperature below T_g. The solid lines in (a) and (b) represent the best fit to Eq. (26).

from Cu nuclei also contribute to muon-spin depolarization. At higher temperatures, $T \sim 3T_g$, where the effect of local fields from Mn moments is eliminated by the fast spin fluctuations, we observed a typical Kubo-Toyabe function $g_z^G(t,\Delta_{Cu})$ of Eq. (8) expected for μ^+ in static nuclear dipolar fields. The observed width $\Delta \sim 0.36\ \mu\text{sec}^{-1}$ of H_{Cu} in *Cu*Mn(1.1 at. %) agreed well with the value for μ^+ in pure Cu. This static line shape confirmed that muons are not diffusing in the crystal up to $t \sim 5\ \mu$sec. Upon cooling towards T_g, the depolarization rate rapidly increased, as shown in Fig. 7, reflecting the slowing-down of random fields H_{Mn} from Mn moments. When the fluctuation of H_{Mn} is relatively fast ($\nu/a \gg 1$), this field works as an independent channel of muon-spin relaxation, in addition to the nuclear dipolar fields. Then the muon-spin-relaxation function should be given by a *product* of the two functions[34] as

$$G_z(t) = \exp[-(\lambda_d t)^{1/2}] g_z^G(t,\Delta_{Cu}) , \tag{25}$$

where

$$g_z^G(t,\Delta_{Cu}) = \tfrac{1}{3} + \tfrac{2}{3}(1-\Delta_{Cu}^2 t^2)\exp(-\tfrac{1}{2}\Delta_{Cu}^2 t^2)$$

[as given by Eq. (8) with $\Delta = \Delta_{Cu}$ for pure Cu]. The data above $T_g = 10.8$ K for *Cu*Mn(1.1 at. %) actually followed this function, as indicated by the solid lines in Fig. 7(a). Below T_g, the initial damping rate of $G_z(t)$ to $\frac{1}{3}$ increased gradually with decreasing temperature [see Fig. 7(b)], while the "tail" of $G_z(t)$ followed the initial damping [see $T = 10$ K in Fig. 7(a)], just as in the case of μ^+ in *Au*Fe. Here the nuclear dipolar field H_{Cu} was decoupled by the larger static field a_s/γ_μ from Mn moments, and had no effect on $G_z(t)$. Consequently, the observed data are very well fitted by a simple form of Eq. (24) [solid lines of Figs. 7(a) and 7(b) below T_g].

An entire time dependence of $G_z(t)$ for *Cu*Mn(5 at. %) is shown in Fig. 8 with very high statistics. In this relatively concentrated specimen, the surface-muon beam was helpful in observing the very quick initial damping of $G_z(t)$. The general features of the results are similar to those for *Cu*Mn(1.1 at. %). As represented by the solid lines in Fig. 8, the observed data fit well to

$$G_z(t) = [G_z(t) \text{ of Eq. (24)}] \times \begin{cases} 1 & \text{for } a_s > \Delta_{Cu} , \\ g_z^G(t,\Delta_{Cu}) & \text{for } a_s \lesssim \Delta_{Cu} , \end{cases} \tag{26}$$

which includes Eq. (25) at $a_s \sim 0$. A slight difference between the observed and fitted shape of $G_z(t)$ at $T = 36$ K suggests that the time correlation of Mn spins in this specimen is somewhat more complicated than the assumed simple form of Eq. (15). The rate of the initial quick damping below T_g increased with decreasing tem-

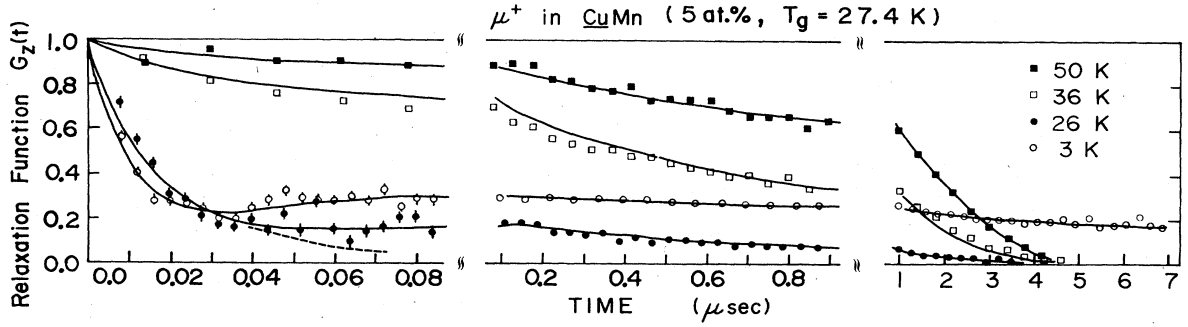

FIG. 8. Zero-field muon-spin-relaxation function observed in *Cu*Mn(5 at. %) ($T_g = 27.4$ K). The high-intensity surface-muon beam at TRIUMF makes it possible to observe very high statistics in the entire time region 4 nsec $\lesssim t \lesssim$ 10 μsec. The solid line represents the best-fit curves for Eq. (26), with the values of a_s and λ_d given in Fig. 10.

perature, and the characteristic "tail" of $G_z(t)$ followed the quick damping, indicating that the static and dynamic local fields from Mn moments coexist at a muon site below T_g. If there were no static component a_s, $G_z(t)$ at $T=26$ K, for example, should have decayed as illustrated by the dashed line in Fig. 8. In this way, in all the specimens of *Au*Fe and *Cu*Mn, the zero-field μSR spectra can be explained by using a simple function of Eq. (24), with no static amplitude ($a_s=0$) above T_g, but with finite values of a_s below T_g.

B. Relaxation functions observed in finite longitudinal fields

In order to study in detail the role of static and dynamic local fields, we also performed a μSR measurement applying finite longitudinal magnetic fields $H_L=0$–640 Oe on *Cu*Mn(1.1 at.%).[15] As shown in Fig. 1 of Ref. 15, the "tail" of $G_z(t)$ increased from ~ 0.3 in zero field to ~ 0.7 in $H_L=640$ Oe at $T=5$ K ($\sim 0.5T_g$), indicating that the static random local fields from Mn moments are decoupled by the applied external fields. The observed spectra at $T=5$ K agreed well with the line shape based on the static relaxation function $g_z^L(t,H_L)$ of Eq. (4) with $a\sim 11$ μsec^{-1}. In contrast, $G_z(t)$ observed above T_g showed almost no dependence on external fields. The effect of nuclear dipolar field H_{Cu} was decoupled in finite longitudinal fields, and the observed spectra followed simple "root-exponential" decay above T_g. These features confirmed that muon spins are depolarized mainly by static random fields at $T\sim 0.5T_g$, and by rapidly fluctuating dynamic random fields above T_g.[15]

We considered further details at $T \lesssim T_g$. In Fig. 9, reproduced from Ref. 16, the field dependence of $G_z(t)$ observed at $T=10$ K ($\sim 0.9T_g$) is compared with the predictions of different model functions. The line shape based on Eqs. (11) and (14), expected for the simple exponential decay of Mn spin correlation, is obviously not adequate. The large field dependence of $G_z(t)$ indicates an important role of static random fields. Next, we tried averaging the simple functions over a probability distribution $P(\nu)$ of the fluctuation rate ν of random fields. This corresponds to the case when the system is divided into large-sized clusters, as mentioned in Sec. III C. The model function in Fig. 9(b), calculated for a Gaussian distribution of $\log_{10}\nu$ having a width $\log_{10}(\Delta\nu)=2$, improved the fit but still is not adequate. When we introduce a wider distribution of ν, the "tail" of $G_z(t)$ for zero field tends to become larger than $\frac{1}{3}$, which does not agree with the observed results. The best fit was obtained when the coexisting static and dynamic local field is assumed, at each muon site, to be a vector sum, as illustrated in Fig. 9(c). Here the solid line represents the calculation for $a_s=4.3$ μsec^{-1} and $\lambda_d=0.6$ μsec^{-1} based on Eq. (17) and its alternative for longitudinal fields. A slight difference from the observed data suggests that the dynamics of the actual system might be somewhat more complicated. Hence, in addition to the results from zero-field μSR, we have another indication from LF μSR that the random field at a muon site in spin glasses can be described by the coexistence of a fast dynamic component and a slow static component below T_g.

C. Amplitude of static random fields

We fitted the observed data for the zero-field relaxation function $G_z(t)$ with Eq. (24) for *Au*Fe and with Eq. (26) for *Cu*Mn, varying a_s and λ_d as the only free parameters. Figure 10(a) shows the temperature dependence of the amplitude a_s of static random local fields determined for *Cu*Mn spin glasses. Although we made no *a priori* as-

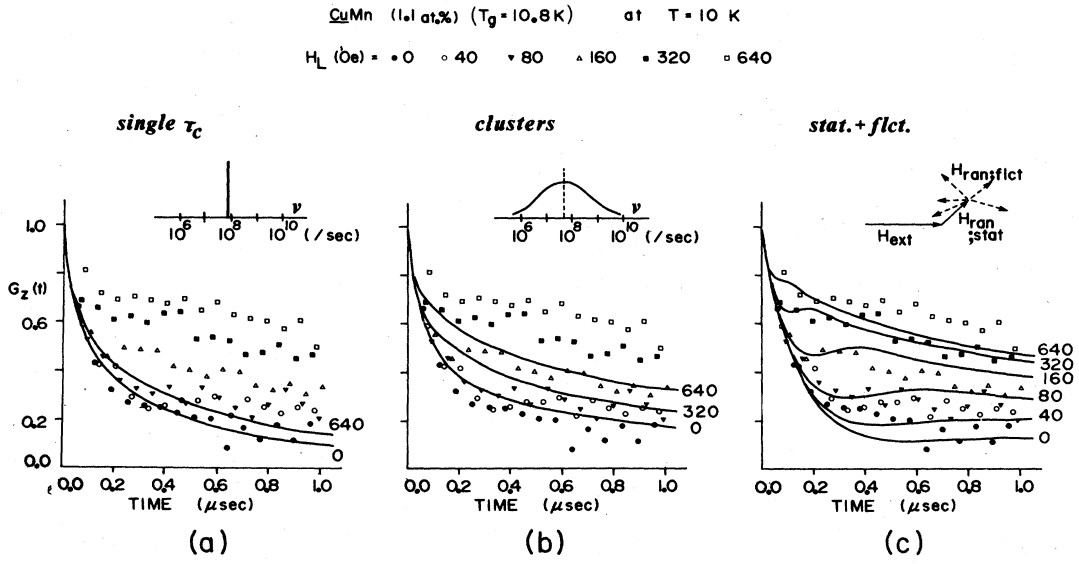

FIG. 9. Muon-spin-relaxation function in *Cu*Mn(1.1 at.%) observed in finite longitudinal magnetic fields $H_L=0$–640 Oe at $T=10$ K ($\sim 0.9T_g$). The field dependence is compared with the predictions of different model functions for different situations in (a)–(c). The best fit to the data among the three was obtained by assuming that static and dynamic local fields coexist as a vector sum at each muon site, as illustrated in (c).

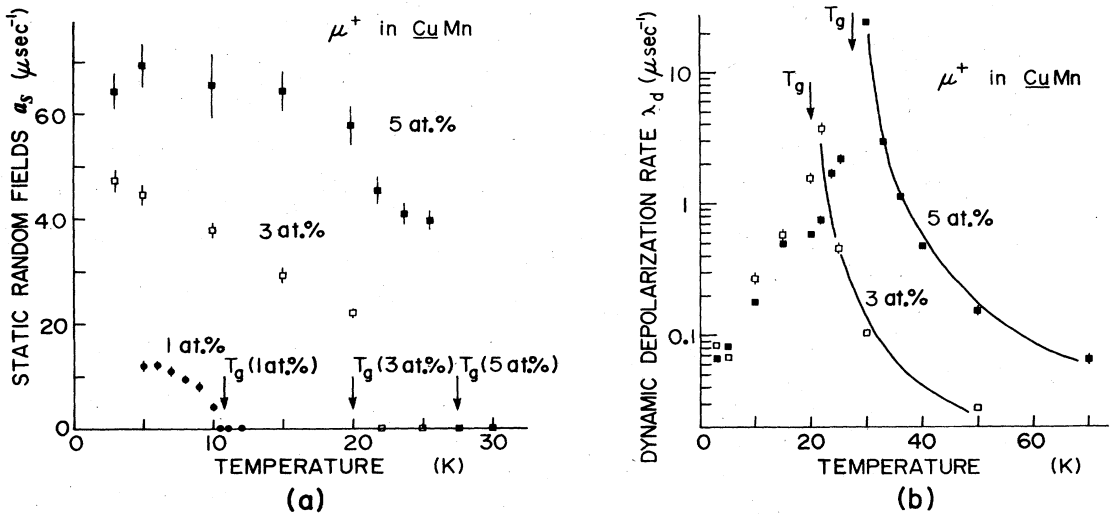

FIG. 10. (a) Static amplitude a_s of random local fields and (b) the dynamic depolarization rate λ_d in *Cu*Mn spin glasses, determined by fitting the observed relaxation function with Eq. (26). a_s becomes finite only below T_g for all the *Cu*Mn samples, and a linear dependence of static random fields on the impurity concentration c is demonstrated in (a). The solid lines in (b) represent the fit of λ_d to the power-law behavior of critical slowing-down, as described in Sec. IV D.

sumptions for the values of a_s above and below T_g, a_s exhibits nonzero values only below T_g of each specimen, indicating the onset of an order parameter below T_g. a_s increases with decreasing temperature towards the full amplitude $a_0=a_s(T=0)$. The experimental results a_0 (5 at.%)$=70$ μsec^{-1} and a_0(3 at.%)$=50$ μsec^{-1} agree reasonably well with the value $a_0=(13-14)\times 100\times c$ μsec^{-1} calculated in Sec. III D for atomic dipolar fields from Mn moments. Figure 11 shows the observed values of a_s for *Cu*Mn(1.1 at.%) (Ref. 35) and *Au*Fe(1.0 at.%) (Ref. 36). In both cases, the amplitude a_s increases smoothly with decreasing temperature towards the theoretical full amplitude [a_0 for *Au*Fe was calculated for atomic dipolar fields from the Fe moment assuming $2\sqrt{S(S+1)}=3.4$ for the Fe moment[2]]. Figure 11 also shows that rough estimates of a_s based on the results of LF μSR in *Cu*Mn(1.1 at.%) at $T=5$ and 10 K are consistent with the values from ZF μSR. The static random field, roughly estimated in *Ag*Mn,[37] shows a tendency similar to the present results.

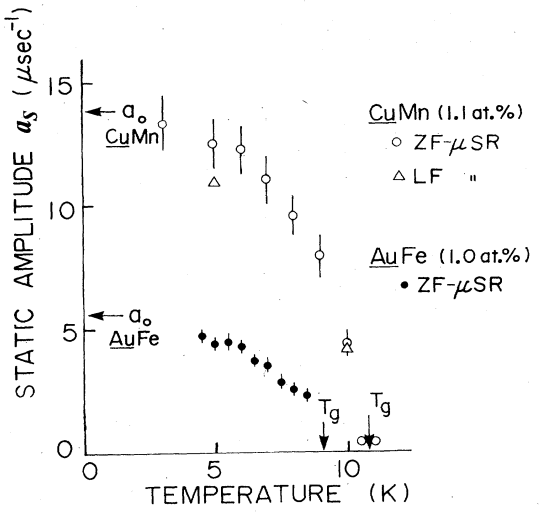

FIG. 11. Static amplitude a_s of random local fields in *Au*Fe(1.0 at.%) ($T_g=9.1$ K) and *Cu*Mn(1.1 at.%) ($T_g=10.8$ K) determined by zero-field μSR. Rough estimates of a_s are also given by longitudinal-field μSR in *Cu*Mn(1.1 at.%). The static amplitude increases with decreasing temperature towards the theoretical full amplitude a_0 calculated in Sec. III D.

These results for a_s in Figs. 10(a) and 11 confirmed that the amplitude of static random fields in dilute-alloy spin glasses is linearly proportional to the concentration c of magnetic impurities, and that the local field at a muon site is due mainly to the atomic dipolar fields. This supports the assumption in Sec. III A that muons occupy all the interstitial sites with equal probability, regardless of the position of magnetic atoms. Since the static amplitude a_s is proportional to the square root of the order parameter Q as $a_s/a_0=\sqrt{Q}$, Figs. 10(a) and 11 represent the static polarization of Mn (or Fe) spins measured by μSR. To cause the quick initial damping of $G_z(t)$, the random field of a_s must be "static" only up to $t\sim 1/a_s\sim 50$–200 nsec. The characteristic "tail" of $G_z(t)$, however, indicates such a field to be static up to $t\sim 1$–5 μsec. Without this persisting field, $G_z(t)$ should have decayed as illustrated by the dashed lines of Figs. 6(c) and 8.

D. Dynamic correlation time

The dynamic depolarization rate λ_d measured in *Cu*Mn(3 at.%) and *Cu*Mn(5 at.%) is shown in Fig. 10(b). Similar results were obtained in *Cu*Mn(1.1 at.%) and in the *Au*Fe specimens. Upon cooling from higher temperatures ($T\sim 3T_g$) towards T_g, λ_d increased rapidly by more than 3 orders of magnitude. Above T_g, where the random fields from the Mn (or Fe) moment have no static com-

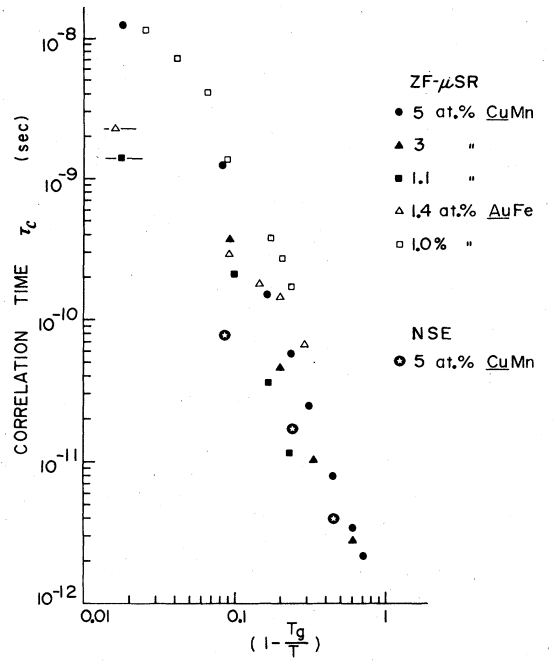

FIG. 12. Correlation time τ_c of Mn (or Fe) moments determined by zero-field μSR from the dynamic depolarization rate observed above T_g. The results for different specimens are plotted versus the reduced temperature scaled with T_g of each specimen. The straight line corresponds to the power law of critical slowing-down. Also plotted is the time $\tau_{\rm NSE}$ when the time correlation function of *Cu*Mn(5 at.%) measured by neutron-spin echo (Ref. 43) decays to $1/e$ as $\xi(\tau_{\rm NSE})=1/e$.

ponent, the amplitude a_d of the dynamic fluctuating field is equal to the full amplitude a_0, as described in Sec. III C. Then, by taking the values of a_0 shown in Figs. 10(a) and 11, we can estimate the fluctuation rate ν of the random fields via the relation $\lambda_d=4a_d^2/\nu$. Assuming that Mn (or Fe) moments and the random fields at muon sites follow the same time evolution, this rate ν also represents the average fluctuation rate of the Mn (or Fe) moment above T_g, and the correlation time τ_c of the Mn (or Fe) moment is given by $1/\nu$. In Fig. 12 the absolute values of τ_c thus obtained for all the specimens of *Cu*Mn and *Au*Fe above T_g are plotted versus the reduced temperature $(T-T_g)/T$. The correlation time increases with decreasing temperature from $\tau_c=10^{-12}$–10^{13} sec at $T\gg T_g$ towards $\tau_c=10^{-8}$–10^{-9} sec at $T\sim T_g$, showing a similar temperature dependence for all the different specimens.

In a plot like Fig. 12, straight lines correspond to the power law

$$\tau_c=\tau_0\left[\frac{T}{T-T_g}\right]^n \tag{27}$$

of critical slowing-down. From the corresponding fit of λ_d to this relation, shown by the solid lines in Fig. 10(b), we obtained the parameters $\tau_0=8\times10^{-13}$ sec and $n=2.9$ for *Cu*Mn(5 at.%), and $\tau_0=7\times10^{-13}$ sec and $n=2.6$ for *Cu*Mn(3 at.%). As indicated by the large values of the power n, the slowing-down of spin fluctuations is very rapid. Note, however, that here the power law may not be the best way to explain the spin dynamics at $T\lesssim1.1T_g$, where the results for τ_c tend to deviate from the straight line extrapolated from higher temperatures. The correlation time τ_c was also compared[13] with the Arrhenius law $\tau_c=\tau_0\exp(E_a/kT)$, and a very large activation energy $E_a\lesssim20kT_g$ was necessary to explain the rapid change of τ_c around T_g. Figure 12 demonstrates that all the results for τ_c can be scaled by using the values of T_g of different specimens. The detailed dependence of τ_c on concentration c is, however, not straightforward, since τ_c of *Cu*Mn(5 at.%) is larger than that of *Cu*Mn(1.1 at.%) at the same reduced temperature, but τ_c of *Au*Fe(1.4 at.%) is smaller than that of *Au*Fe(1.0 at.%) in a similar comparison. The absolute values and the temperature dependence of τ_c agree reasonably well with the zero-field μSR results for *Ag*Mn,[37] as was pointed out.[16,37]

As shown in Fig. 10(b), the dynamic depolarization rate decreases with decreasing temperature below T_g. Similar temperature dependence was obtained in *Cu*Mn(1.1 at.%) below T_g,[35] and these results are also consistent with those for *Ag*Mn (Ref. 37) below T_g. Since the static amplitude a_s of random fields becomes finite below T_g, the dynamic amplitude a_d is substantially changed from the full amplitude a_0 as $a_d^2=a_0^2-a_s^2$. Thus the change in $\lambda_d=4a_d^2/\nu$ should be due partly to a rapid decrease of a_d below T_g. As seen in Figs. 10(a) and 11, it is not possible to estimate a_d^2 accurately, especially at lower temperatures where $a_s\sim a_0$. Therefore, we present here only the values $\tau_c=1.7\times10^{-10}$ sec at $T=26$ K and $\tau_c=9.1\times10^{-11}$ sec at $T=20$ K for *Cu*Mn(5 at.%) as rough estimates of τ_c below T_g. Upon cooling from T_g, τ_c decreases slowly and reaches around 10^{-10}–10^{-11} sec at $T\sim0.5T_g$ in all the specimens. The rate $\nu=1/\tau_c$ below T_g describes the average decay rate of the Mn spin correlation function $\xi(t)$ from $\xi(t)=1$ at $t=0$ towards the static order parameter $\xi(t)=Q=(a_s/a_0)^2$ at $t\sim1$ μsec. In this way, we obtained the static spin polarization as well as the average decay rate of impurity spin correlation in spin glasses above and below T_g by zero-field μSR.

V. COMPARISON WITH RESULTS OF OTHER EXPERIMENTAL TECHNIQUES

A. Mössbauer effect

The static random local field a_s of ZF μSR can be directly compared with the static hyperfine field $H_{\rm hf}$ measured by Mössbauer effect (ME) since both (a_s/a_0) and $H_{\rm hf}(T)/H_{\rm hf}(T=0)$ are linearly proportional to the static spin polarization of Fe moment below T_g. In Fig. 13 the present μSR results for *Au*Fe(1.0 at.%) are compared with $H_{\rm hf}$ values of ^{57}Fe ME measured by Violet and Borg[38] in *Au*Fe spin glasses of various concentrations. The observed results of the different techniques agree well when the temperature is scaled with T_g. The "static" spin polarization of Fe moments increases rapidly as the temperature is decreased from T_g. The dividing time scale between "static" and "dynamic" corresponds to $t=1/a_s=10^{-7}$–10^{-6} sec for ZF μSR and

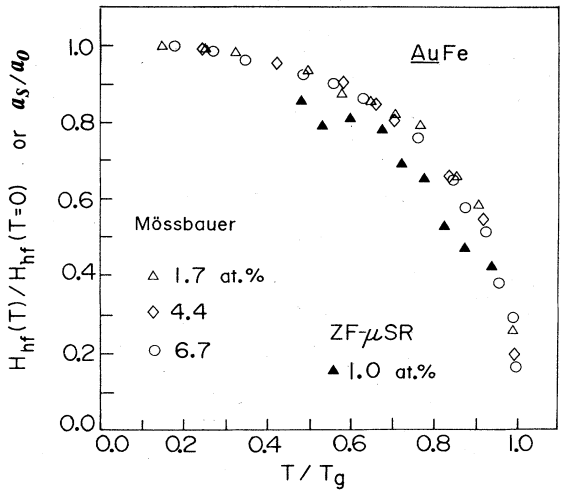

FIG. 13. Comparison of the present zero-field μSR results for a_s/a_0 in *Au*Fe(1.0 at. %) with the static hyperfine field H_{hf} measured by ^{57}Fe Mössbauer-effect experiments in various *Au*Fe specimens by Violet and Borg (Ref. 38).

$t=10^{-7}$–10^{-8} sec for ^{57}Fe ME. The line shape of the Mössbauer effect was analyzed assuming the static contribution only, whereas we also took into account the dynamic effect in ZF μSR via the relaxation function of Eq. (24) below T_g. In this respect, ZF μSR provides somewhat more accurate information about static spin polarization, especially at temperatures close to T_g.

B. ac susceptibility

The ac susceptibility χ_{ac} of dilute-alloy spin glasses exhibits a sharp cusp at T_g. The curvature of χ_{ac} above T_g follows the Curie law,

$$\chi_{ac}=C/kT\equiv\chi_{Curie}(T)\ . \tag{28}$$

The Curie constant C keeps the single-spin value for low-concentration ($\sim$1 at. %) samples up to high temperatures, while a short-range ferromagnetic coupling among 2–3 neighboring Mn moments makes C considerably larger than the single-spin value per atom for *Cu*Mn(5 at. %) near T_g. In the following, we use the Curie constant derived from the data on χ_{ac} just above T_g. If spins kept fluctuating much faster than the measuring frequency ω_{meas} of χ_{ac} even below T_g, then χ_{ac} should have increased with decreasing temperature, following the extrapolated Curie law in all the specimens. The sudden reduction of χ_{ac} below T_g can thus be attributed to the onset of "static" polarization of impurity spins persisting up to $t\gtrsim 1/\omega_{meas}$.

Since the susceptibility is quadratically proportional to the responding dynamic component of the spin system, the reduction of $\chi_{ac}(T)$ from $\chi_{Curie}(T)$ below T_g directly corresponds to the static order parameter $Q(T)$ as

$$\mathrm{Stat}[\chi_{ac}](T)\equiv\frac{\chi_{Curie}(T)-\chi_{ac}(T)}{\chi_{Curie}(T)}=Q(T) \tag{29}$$

determined at the time window $t\sim 1/\omega_{meas}$. In Figs. 14(a) and (b) the above quantity Stat$[\chi_{ac}](T)$ measured by Chikazawa *et al.*[39] is compared with the present ZF μSR results for $(a_s/a_0)^2$ in *Au*Fe(1.0 at. %) and *Cu*Mn(1.1 at. %). Cut-off pieces of the same specimens were used for the different techniques. The values of static order parameter Q determined by μSR at $t\sim 1/a_s\sim 0.1$–1 μsec and by χ_{ac} at $t\sim 1/\omega_{meas}=50$ msec agree reasonably well for both specimens. This suggests that the static polarization persists from $t\sim 0.1$ μsec to $t\sim 50$ msec, keeping a rather constant value in time below T_g.

Such a comparison of susceptibility-type measurements (χ_{ac}, neutron scattering) with hyperfine-field–type measurements (μSR, ME) brings out another fundamental feature of random systems. The response of the ith spin in Stat$[\chi_{ac}]$ and that in "elastic ($\Delta E=0$)" intensity I_{el} of

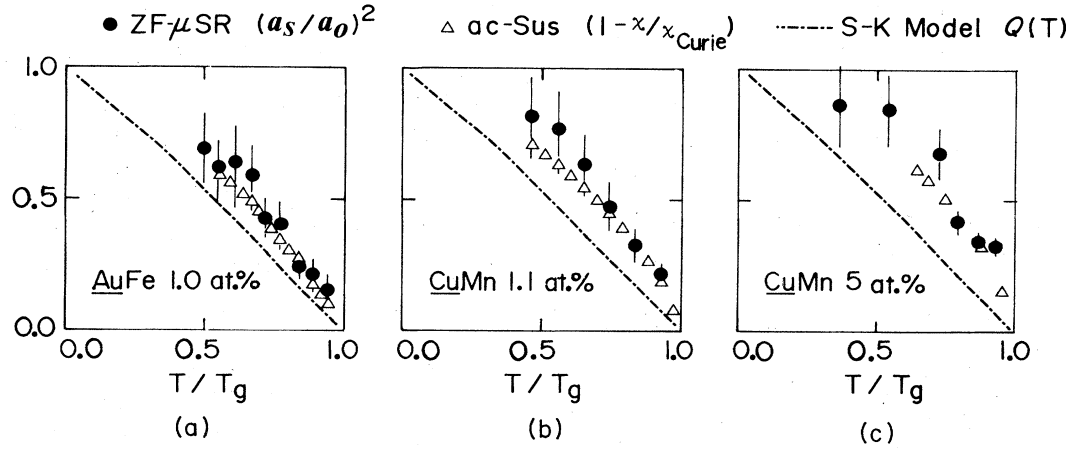

FIG. 14. Comparison of $(a_s/a_0)^2$ measured by zero-field μSR with the order parameter $Q(T)=[1-\chi_{ac}(T)/\chi_{Curie}(T)]$ determined by ac susceptibility, χ_{ac}, measured on cut-off pieces of the same specimens. χ_{ac} was measured for *Au*Fe(1.0 at. %) and *Cu*Mn(1.1 at. %) by Chikazawa *et al.* (Ref. 39) with $\nu=80$ Hz, and for *Cu*Mn(5 at. %) by Tholence (Ref. 45) with $\nu=10$ Hz. The dashed line represents a theoretical calculation of $Q(T)$ for an infinite-ranged Ising model of Kirkpatrick and Sherrington (Ref. 49); this dashed line is also checked to agree well with the computer simulation for RKKY spin glasses made by Walker and Walstedt (Ref. 42).

neutron scattering are both quadratically proportional to the thermally averaged static polarization $P_i=(Q_i)^{1/2}$ of the ith spin. Then the response from the entire system can be given by

$$\text{Stat}[\chi_{\text{ac}}] \text{ or } I_{\text{el}}/I_{\text{el}}(T=0)=\langle P_i^2\rangle_i=\langle Q_i\rangle_i \ , \tag{30}$$

where $\langle\ \rangle_i$ denotes the spatial average over different spins. On the other hand, the static random field a_s is linearly proportional to spin polarization as

$$a_s/a_0=\langle P_i\rangle_i \ . \tag{31}$$

If all the spins have the same values of P_i (or Q_i), as illustrated in Fig. 15(a), then we expect the relation $\text{Stat}[\chi_{\text{ac}}](T)=Q(T)=(a_s/a_0)^2$. We will denote this picture "homogeneous freezing." In contrast, when some of the individual spins are completely frozen ($P_i=1$), while the rest are fluctuating rapidly $P_i=0$ as illustrated in Fig. 15(b), both the susceptibility $\text{Stat}[\chi_{\text{ac}}]$ and the hyperfine field are linearly proportional to the number of frozen ($P_i=1$) spins. Then $\text{Stat}[\chi_{\text{ac}}](T)=Q(T)=(a_s/a_0)$. We denote this picture "inhomogeneous individual freezing."

Therefore, by comparing (a_s/a_0) or $(a_s/a_0)^2$ with $\text{Stat}[\chi_{\text{ac}}]$ or I_{el} of neutrons, we can distinguish these two pictures of spin freezing and investigate the degree of difference for P_i among different individual spins. This benefit of such a comparison was originally pointed out by Uemura,[40] and has been described in Refs. 36 and 41.

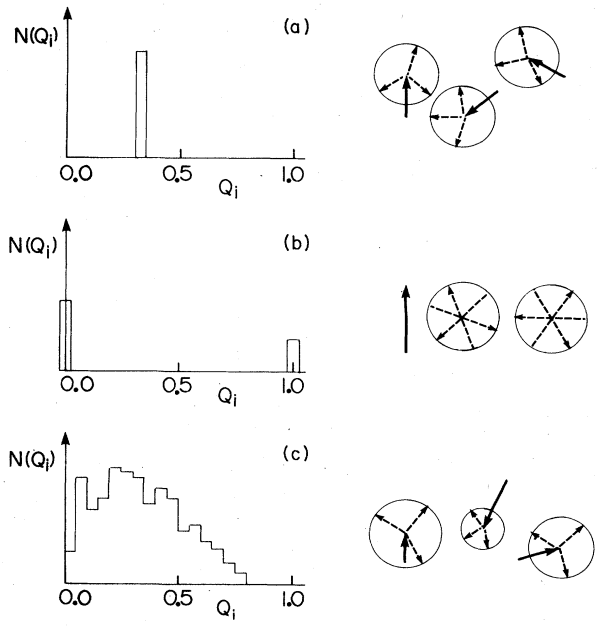

FIG. 15. Schematic illustration of various types of spin freezing in spin glasses below T_g. (a) All the impurity spins have equal static polarization; this is "homogeneous freezing." (b) Some individual spins are completely frozen ($Q_i=1$), while the rest are fluctuating ($Q_i=0$); this is "inhomogeneous individual freezing." (c) Computer-simulation results of Walker and Walstedt (Ref. 42) for 960 individual spins. With the spatial average over different spins denoted by $\langle\ \rangle_i$, (a)—(c) are all drawn for $\langle Q_i\rangle_i=0.33$. The quantity $[\langle(Q_i)^{1/2}\rangle]^2$, however, becomes 0.33 for (a), 0.11 for (b), and 0.30 for (c).

The good agreement obtained in the quadratic comparison of $\text{Stat}[\chi_{\text{ac}}]$ with $(a_s/a_0)^2$ in Fig. 14 indicates that the actual system behaves more like the "homogeneous freezing" model. Note, however, that the relation

$$\langle Q_i\rangle_i=[\langle(Q_i)^{1/2}\rangle_i]^2 \ ,$$

expected for the homogeneous freezing, works as a good approximation even for a relatively wide variety of P_i and Q_i, as illustrated in Fig. 15(c). This figure represents the population distribution of the order parameter Q_i among 960 individual spins with $\langle Q_i\rangle_i=0.33$ obtained in a computer-simulation study by Walker and Walstedt[42] below T_g. The quantity $[\langle(Q_i)^{1/2}\rangle_i]^2$ becomes 0.30 for this distribution. Within the experimental accuracy, the present results in Fig. 14 are then consistent even with such a wide variety of Q_i. All the three distributions at different temperatures given in Fig. 4 of Ref. 42 have been checked to be consistent with the present results. Nevertheless, we can clearly rule out the very "inhomogeneous freezing" such as in Fig. 15(b), since a_s/a_0 (Fig. 13) shows a distinctly different temperature dependence from that of $\text{Stat}[\chi_{\text{ac}}](T)$ in Fig. 14. If "inhomogeneous freezing" were the case, the points for ZF μSR in Fig. 14 should be much lower than the points for χ_{ac}.

When the dynamic ($Q_i=0$) spins are fluctuating very fast ($\nu/a\gg1$) and when the frozen ($Q_i=1$) spins are distributed in a microscopically random way in the "inhomogeneous freezing" model of Fig. 15(b), the muon-spin-relaxation function $G_z(t)$ is expected to have a shape similar to Eq. (17) obtained for the "homogeneous freezing." Therefore, the line shape of ZF μSR data alone does not provide information sufficient for a clear distinction between the two different pictures of spin freezing. As described in this section, it is the comparison of the results from the two different experimental techniques that allowed us to investigate the different types of spin freezing below T_g.

C. Neutron-spin echo

Mezei and Murani[43] performed a neutron-spin-echo (NSE) measurement with the same specimen of *Cu*Mn(5 at. %) used in the present μSR experiment, and directly obtained the time correlation function $\xi(t)$ of Mn moments at $t\lesssim10^{-9}$ sec from the elastic intensity I_{el} of magnetic neutron scattering, as shown in Fig. 16. The ac susceptibility χ_{ac} was also measured with the same specimen using a few different measuring frequencies ω_{meas}, and the static order parameter was plotted at $t=1/\omega_{\text{meas}}$ by Murani *et al.*[44] to extend the time region of $\xi(t)$. In order to compare the static spin polarization measured by ZF μSR below T_g, we plotted $(a_s/a_0)^2$ of *Cu*Mn(5 at. %) at $t=1/a_s$ for $T=26$ and 20 K in Fig. 16. The attached dashed lines indicate the persistency of the static component expected from the characteristic "tail" of the muon relaxation function $G_z(t)$ observed at these temperatures. The results of ZF μSR nicely cover the time region between those of NSE and χ_{ac}. The smooth connection of $(a_s/a_0)^2$ to I_{el} and $\text{Stat}[\chi_{\text{ac}}]$ suggests that the spin freezing is "homogeneous" also in *Cu*Mn(5 at. %). This feature can also be found in a detailed comparison of the

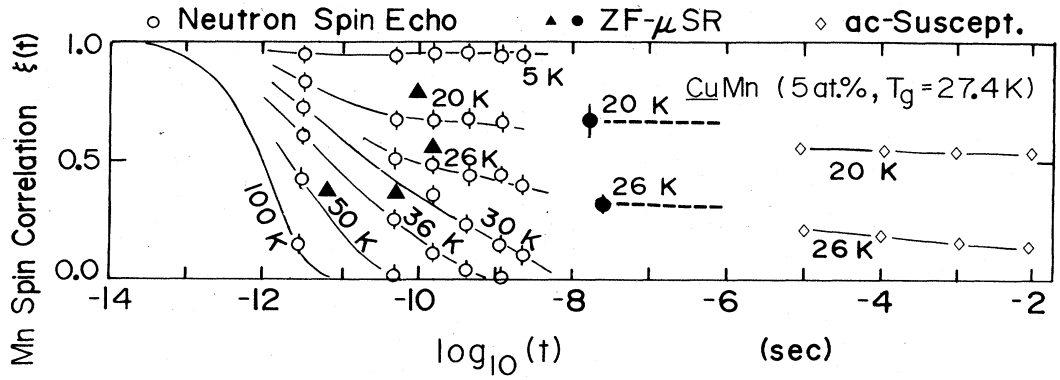

FIG. 16. Comparison of the time correlation $\xi(t)$ of the Mn moment in *Cu*Mn(5 at. %) measured by neutron-spin echo (NSE) (Ref. 43), zero-field μSR (ZF μSR), and ac susceptibility (χ_{ac}) (Ref. 44). The triangle points for ZF μSR are plotted at $\xi(t=\tau_c)=1/e$ at $T=50$ and 36 K (above T_g), and at $\xi(t=\tau_c)=(1-Q)/e+Q$ with $Q=(a_s/a_0)^2$ at $T=26$ and 20 K, by using the dynamic correlation time τ_c obtained in Sec. IV D. The solid circles are plotted to represent the static spin polarization at $\xi(1/a_s)=(a_s/a_0)^2$ at $T=26$ and 20 K, and the attached dashed lines indicate the persistency of this polarization expected from the characteristic "tail" of $G_z(t)$ observed in ZF μSR.

results from χ_{ac} [measured at 10 Hz (Ref. 45)] and those from ZF μSR for *Cu*Mn(5 at. %) shown in Fig. 14(c). At $T=26$ K, just below $T_g=27.4$ K, $\xi(t)$ decreases slowly after $t\sim10^{-9}$ sec, which indicates that the spin polarization is not perfectly "static" in this specimen near T_g. This is in a clear contrast to the results for lower-concentration ($c\sim1$ at. %) specimens, for which $(a_s/a_0)^2=\mathrm{Stat}[\chi_{ac}]$ even at $T\sim T_g$.

We can also compare the dynamic decay rate of $\xi(t)$ measured by NSE and μSR above and below T_g. Since only the average correlation time τ_c can be determined by ZF μSR without detailed information on the shape of $\xi(t)$ above T_g, we plotted the points at $\xi(t=\tau_c)=1/e$ for $T=50$ and 36 K in Fig. 16 as representative of μSR results above T_g. To compare the decay rate below T_g, we also plotted

$$\xi(t=\tau_c)=(a_s/a_0)^2+[1-(a_s/a_0)^2](1/e)$$

with the values of τ_c and a_s at $T=26$ and 20 K given in IV C and IV D. These points roughly agree with the results of NSE. To make a more detailed comparison, we found the time τ_{NSE} when the correlation function of NSE decays into $1/e$ as $\xi(\tau_{NSE})=1/e$ by using the NSE data in Fig. 16 above T_g, and compared it with the correlation time of ZF μSR in Fig. 12. The values from NSE and ZF μSR for the same *Cu*Mn(5 at. %) roughly agree at higher temperatures, but ZF μSR gives a longer correlation time than NSE at $T\sim T_g$. This may be due to the significant deviation of $\xi(t)$ from the simple form of Eq. (15) around T_g found by NSE, since a relatively small number of "slower spins" make a large contribution to muon relaxation when there is a "microscopic" distribution of correlation times τ_c among different spins.

The uniform susceptibility χ_{ac} probes the dynamics at the wave-vector component $q=0$, NSE probes around $q=0.1$ Å^{-1}, and the μSR results reflect the integrated information over all the q components in the Brillouin zone since a positive muon is a pointlike magnetic probe. The NSE measurements on *Cu*Mn(5 at. %) with $q=0.1$ and 0.4 Å^{-1} exhibited the same temperature dependence,[46] and indicated that the dynamics do not depend much on q for smaller q values. Recently, Uemura and Shapiro[47] performed an inelastic-neutron-scattering experiment on a different single-crystal sample of *Cu*Mn(5 at. %) and found that the temperature variation of the scattering intensity does not depend much on q up to $q\sim3$ Å^{-1}. In this measurement, the spatial spin correlation of *Cu*Mn(1.1 at. %) (the same specimen used in the present μSR experiment) was found to be completely random in orientation.[47,41] These results suggest that spin freezing in *Cu*Mn spin glasses (for $c\lesssim5$ at. %) occurs roughly with the same time correlation for all q components, thus providing a basis for the direct comparison of the three different techniques. The overall agreement between the zero-field results from NSE, ZF μSR, and χ_{ac} in Figs. 14 and 16 is very good, and this gives general support to the reliability of these techniques in probing the dynamics of spin glasses. The combined time correlation function in Fig. 16 demonstrates rapid slowing-down of Mn moments above T_g, and the onset of persisting "quasistatic" spin polarization below T_g.

VI. DISCUSSION AND CONCLUSIONS

In the preceding section we ruled out the "inhomogeneous individual freezing" model. An example of such "inhomogeneous" freezing can be found in a percolation-like picture of spin-glass freezing. Here the reduction of χ_{ac} below T_g is attributed to the increasing population of individual spins joining an infinite cluster of frozen ($Q_i=1$) spins, i.e., expansion of the infinite cluster with decreasing temperature below T_g. The present results suggest that spin freezing takes place in a much more cooperative fashion, and that the dynamic response of χ_{ac} below T_g is due not to a small population of "free spins," but rather to the majority of impurity spins in the system.

The dashed line in Fig. 14 shows the mean-field calculation of order parameter $Q(T)$ for an infinite-ranged Ising model of Kirkpatrick and Sherrington.[49] This model effectively connects an infinite number of spins and thus

represents the most "cooperative" and "homogeneous" spin freezing. Its result for $Q(T)$ agrees well with the computer simulation of Walker and Walstedt for RKKY spin glasses in Fig. 4 of Ref. 42. The observed results from χ_{ac} and ZF μSR for *Au*Fe(1.0 at. %) give slightly larger values of $Q(T)$ than do such theoretical and computer results at the same reduced temperature. This deviation becomes more pronounced for *Cu*Mn(5 at. %), especially around $T \sim T_g$. Consequently, Fig. 14 indicates that the lower-concentration dilute alloys are closer to the idealized situation of canonical spin glasses.

In fact, neutron-scattering studies have revealed that the orientations of spins are actually random for low-concentration ($c \lesssim 2$ at. %) alloys,[50] but a short-range ferromagnetic interaction couples a few neighboring moments in *Cu*Mn(5 at. %) and other concentrated systems.[50] Furthermore, Cable *et al.*[51] recently reported that some of the spins form a relatively long-range ordering of spin-density waves in concentrated *Cu*Mn systems ($c = 5$—25 at. %). These complicated local magnetic structures and couplings would be a principal factor in making $Q(T)$ in *Cu*Mn(5 at. %) different from that in the simple mean-field model. Indeed, ferromagnetic coupling tends to make the rise of $Q(T)$ at $T \sim T_g$ sharper than in idealized spin glasses, as indicated in Ref. 49. In this respect, it should be interesting to compare the $Q(T)$ of many different types of spin glasses, including amorphous aluminosilicate glasses, $(Eu_xSr_{1-x})S$, etc. It would also be important to simulate "very inhomogeneous freezing," such as in Fig. 15(b), to calculate $Q(T)$, and to compare it with the experimental results.

Assuming the scaling argument of low-concentration canonical spin glasses[52] for T, H, and c, we would expect $\tau_c T_g$ to be an invariant quantity for different concentrations at a given normalized temperature.[53] As shown in Fig. 12, however, this relation is not necessarily obeyed for *Cu*Mn spin glasses (1—5 at. %), for which the value of $\tau_c T_g$ increases with increasing concentration. We have also seen that the time correlation $\xi(t)$ of Mn moments in *Cu*Mn(5 at. %) shows a slow gradual decay at $t \gtrsim 10^{-9}$ sec at $T = 26$ K, just below T_g. These features might well be attributable to the complicated local situation of the higher-concentration specimen.

The neutron-spin-echo experiment showed a deviation of $\xi(t)$ in *Cu*Mn(5 at. %) from the simple form of Eq. (15). Theoretically, several models have been proposed for the shape of time correlation function $\xi(t)$. An algebraic decay $\xi(t) \sim t^{-\eta}$ was postulated by Sompolinsky *et al.*[54] This shape roughly agrees with the NSE results around T_g, but has a difficulty since $\xi(t)$ diverges for $t \to 0$, and, consequently, the power spectrum of spin fluctuations cannot be normalized to absolute values. "Stretched exponential" shape $\xi(t) = \exp[-(\Lambda t)^{1-\beta}]$ has been considered by Nagi *et al.* and Arrott *et al.*,[55] and has recently been found to explain the time dependence of remanent magnetization below T_g.[56] The deviation from the simple exponential shape can be attributed to the different local environment of each spin, and the "root-exponential" shape of $G_z(t)$ given in Sec. III B actually represents a typical "stretched exponential" function. It is, however, not easy to reproduce the observed shape of $\xi(t)$ at $T \sim T_g$ with the stretched exponential function. At $T = 26$ K, for example, a large stretching constant β is needed to account for the slow decay of $\xi(t)$ at $t \gtrsim 10^{-8}$ sec, but then it becomes difficult to explain the relatively quick decay of $\xi(t)$ at $t \lesssim 10^{-10}$ sec.

As described in Sec. III C, the time correlation function $\xi_H(t)$ of random fields H at muon sites is not necessarily the same as the spin correlation function $\xi_S(t)$, especially when $\xi_S(t)$ has a complicated shape. Moreover, the effect of the complicated spin structure of *Cu*Mn(5 at. %) on $\xi_H(t)$ is unclear at present. Therefore, it is not possible to obtain theoretical forms of $G_z(t)$ expected for complicated time and spatial spin correlations. Under such circumstances we have employed the simpler form of Eq. (24) for the muon-spin-relaxation function $G_z(t)$ in this paper.[57] We avoid the use of overly complicated and unreliable model functions. Equation (24) allows us to compare the results for different specimens from the same standpoint, free from any *a priori* assumptions. The agreement of the assumed line shapes of Eq. (24) with the data was very good, as shown in Figs. 6—8.

In the present approach we tried to obtain only the average quantities a_s and τ_c. The spirit here is very similar to the mean-field approximation, wherein one deals only with the averaged physical quantities. The "homogeneous" freezing of impurity moments found in Secs. V B and V C suggests that the observed quantity of a_s represents the majority of spins. The local field H at a muon site reflects several neighboring magnetic moments, and the possibly different time correlations of individual spins are somewhat averaged at each muon site. These features provide support for the present approach. The good agreement obtained in the comparisons with other techniques confirmed that ZF μSR is a very good tool for probing such average quantities.

It is, however, difficult for μSR to directly determine the shape of $\xi(t)$, which is a quantity beyond the mean-field-like picture. Recently, an attempt was made by MacLaughlin *et al.*[58] with LF μSR in *Ag*Mn applying high external fields up to $H_L = 5$ kG. The spectral distribution of the fluctuating field below T_g was "gated" by the Zeeman level $\omega = \gamma_\mu H_L$, and an algebraic time dependence of $\xi(t)$ was reported.[58] Although this is a good step forward, the information is not free from the possible change of dynamics of the spin system itself under a high applied field. Moreover, the studied time region is limited within $\omega \lesssim \gamma_\mu H_L$, $t \gtrsim 10^{-9}$ sec, which is only the "tail end" of the frequency spectrum of the dynamic component. Therefore, at present, neutron-spin echo is a much more direct and powerful tool than μSR for investigating the detailed shape of $\xi(t)$ at $t \lesssim 10^{-9}$ sec. In this respect, it is very important to accumulate accurate data on NSE for low-concentration dilute alloys[59] which are not affected by the complicated spatial spin correlation.

In summary, we have developed a stochastic theory of muon-spin relaxation in dilute-alloy spin glasses, and obtained an analytic form of Eq. (17) for the zero-field muon-spin-relaxation function expected in coexisting static and dynamic random fields from impurity moments. Detailed measurements of zero-field μSR have been performed in *Au*Fe and *Cu*Mn, mainly with the high-

intensity surface-muon beam, and the observed results are well explained by the theoretical form of Eq. (17). The characteristic "root-exponential" decay of $G_z(t)$, expected for the case of no static fields, has been observed above T_g. The line shapes of ZF and LF μSR below T_g clearly indicated the coexistence of static and dynamic random fields at each muon site. Using the spatial averaging function $\rho(\Delta)$ of Eq. (9), a convenient "sum rule" was presented to calculate the average amplitude of random local fields. The observed full amplitude of random fields showed linear dependence on concentration c, and agreed well with the above theoretical calculation for atomic dipolar fields.

The static amplitude a_s of random fields attained finite values only below T_g, and increased with decreasing temperature towards the full amplitude a_0. The temperature dependence of a_s/a_0 agreed well with the results of Mössbauer spectroscopy, and $(a_s/a_0)^2$ agreed with the order parameter $Q(T)$ measured by ac susceptibility. Thanks to the fundamental difference between the different experimental methods, the comparisons of ZF μSR with χ_{ac} and NSE have ruled out the extremely inhomogeneous spin freezing of Fig. 15(b). They have indicated that the magnetic moments in spin glasses have a rather homogeneous amplitude of the frozen component below T_g, as illustrated in Figs. 15(a) or Fig. 15(c). The dynamic correlation time τ_c of Mn (or Fe) moments, determined by ZF μSR in all the specimens above T_g, showed rapid slowing-down of spin fluctuations from $\tau_c \sim 10^{-12}$ sec at $T > 2T_g$ towards $\tau_c \sim 10^{-9}$ sec at $T \sim T_g$. The values of τ_c measured in *Cu*Mn(5 at. %) by μSR roughly agreed with neutron-spin echo above and below T_g. The time correlation function $\xi(t)$ of Mn spins in *Cu*Mn(5 at. %) has been given in an entire time range of 10^{-12}—10^{-2} sec by connecting the results of NSE, ZF μSR, and χ_{ac}. ZF μSR has provided detailed information on spin dynamics in the time region inaccessible for NSE and χ_{ac}. The combined information from the three methods in *Au*Fe and *Cu*Mn spin glasses has demonstrated rapid slowing-down of impurity spins above T_g and the appearance of long-time, persisting static spin polarization below T_g.

ACKNOWLEDGMENTS

The authors would like to thank H. Miyajima for preparing the specimens of *Au*Fe and *Cu*Mn(1.1 at. %); A. P. Murani for providing the specimens of *Cu*Mn(3 at. %) and *Cu*Mn(5 at. %) and for participating in the μSR measurement; S. Chikazawa, Y. Miyako, and J. L. Tholence for measuring the ac susceptibility of the specimens; R. S. Hayano, K. Nishiyama, J. Imazato, and C. Y. Huang for their help in the early stages of the present study; V. Jaccarino, R. Kubo, and F. Mezei for stimulating discussions; J. H. Brewer, C. W. Clawson,, and K. M. Crowe for the development of the surface-muon facilities at TRIUMF; and E. W. Vogt for hospitality at TRIUMF. One of us (Y.J.U.) would like to thank G. Shirane and S. M. Shapiro for their hospitality at Brookhaven National Laboratory (BNL); S. M. Shapiro for collaboration on the neutron-scattering work; and the Japan Society for the Promotion of Science Foundation for financial support to perform research abroad. The present work was supported by the Japan Society for the Promotion of Science Foundation and by the National Science and Engineering Research Council (NSERC) of Canada, and the study at BNL was supported by the Division of Materials Science, U. S. Department of Energy, under Contract No. DE-AC02-76CH00016. Part of the present study is based on the Ph.D. thesis of Y. J. Uemura at the University of Tokyo, 1982.

---

*On leave from Department of Physics, University of Saskatchewan, Saskatoon, Saskatchewan, Canada S7N 0W0.

[1]For a review of experimental studies, see J. A. Mydosh, J. Magn. Magn. Mater. **7**, 237 (1978); J. A. Mydosh, presented at *Heidelberg Colloquium on Spin Glasses, 1983,* edited by J. L. van Hemmen and I. Morgenstern (Springer, Heidelberg, 1983).

[2]For a reivew of theoretical studies, see A. Blandin, J. Phys. (Paris) Colloq. **39**, C6-1499 (1978).

[3]V. Cannella and J. A. Mydosh, Phys. Rev. B **6**, 4220 (1972).

[4]J. L. Tholence and R. Tournier, J. Phys. (Paris) Colloq. **35**, C4-229 (1974).

[5]S. F. Edwards and P. W. Anderson, J. Phys. **F5**, 965 (1975), **6**, 1927 (1976).

[6]For general aspects of muon-spin relaxation, see the following three proceedings of international conferences on muon-spin rotation: Hyperfine Interact. **6** (1979); **8** (1981); **17-19** (1984).

[7]D. E. Murnick, A. T. Fiory, and W. J. Kossler, Phys. Rev. Lett.**36**, 100 (1976).

[8]K. Emmerich and Ch. Schwink, Hyperfine Interact. **8**, 767 (1981).

[9]J. A. Brown, R. H. Heffner, T. A. Kitchens, M. Leon, C. E. Olsen, M. E. Schillaci, S. A. Dodds, and D. E. MacLaughlin, J. Appl. Phys. **52**, 1766 (1981).

[10]D. E. MacLaughlin and H. Alloul, Phys. Rev. Lett. **36**, 1158 (1976); **38**, 181 (1977); D. A. Levitt and R. E. Walstedt, *ibid.* **38**, 178 (1977).

[11]E. D. Dahlberg, M. Hardiman, R. Orbach, and J. Soulete, Phys. Rev. Lett. **42**, 401 (1979); M. B. Salamon, Solid State Commun. **31**, 781 (1979).

[12]Y. J. Uemura, Hyperfine Interact. **8**, 739 (1981).

[13]An early stage of the present study was briefly reported in Y. J. Uemura, T. Yamazaki, R. S. Hayano, R. Nakai, and C. Y. Huang, Phys. Rev. Lett. **45**, 583 (1980).

[14]The experiments on *Cu*Mn(3 at %) and *Cu*Mn(5 at. %) samples have been performed by Y. J. Uemura, D. R. Harshman, M. Senba, E. J. Ansaldo, and A. P. Murani, Phys. Rev. B **30**, 1606 (1984).

[15]Y. J. Uemura, K. Nishiyama, T. Yamazaki, and R. Nakai, Solid State Commun. **39**, 461 (1981).

[16]Y. J. Uemura and T. Yamazaki, Physica **109&110B**, 1915 (1982).

[17]R. S. Hayano, Y. J. Uemura, J. Imazato, N. Nishida, K. Nagamine, T. Yamazaki, and H. Yasuoka, Phys. Rev. Lett. **41**, 421 (1978).

[18]Y. J. Uemura, R. S. Hayano, J. Imazato, N. Nishida, and T. Yamazaki, Solid State Commun. **31**, 731 (1979); R. S. Hayano, Y. J. Uemura, J. Imazato, N. Nishida, T. Yamazaki, and

R. Kubo, Phys. Rev. B **20**, 850 (1979).
[19]R. S. Hayano, Y. J. Uemura, J. Imazato, N. Nishida, K. Nagamine, T. Yamazaki, H. Yasuoka, and Y. Ishikawa, Phys. Rev. Lett. **41**, 1743 (1978).
[20]J. H. Brewer, Hyperfine Interact. **8**, 831 (1981).
[21]C. A. M. Mulder, A. J. van Deyneveldt, and J. A. Mydosh, Phys. Rev. B **23**, 1384 (1981).
[22]O. Hartmann, Hyperfine Interact. **6**, 203 (1979); C. W. Clawson, K. M. Crowe, S. S. Rosenblum, S. E. Kohn, C. Y. Huang, J. L. Smith, and J. H. Brewer, Phys. Rev. Lett. **51**, 114 (1983); R. Kadono, J. Imazato, K. Nishiyama, K. Nagamine, T. Yamazaki, D. Richter, and J. M. Walter, Hyperfine Interact. **17-19**, 109 (1984).
[23]M. Camani, F. N. Gygax, W. Ruegg, A. Schenck, H. Schilling, E. Klempt, R. Schylze, and H. Wolf, Phys. Rev. Lett. **42**, 679 (1979).
[24]C. H. Townes, C. Herring, and W. D. Knight, Phys. Rev. **77**, 852 (1950).
[25]The static width of the Ruderman-Kittel-Kasuya-Yosida (RKKY) field on Cu nuclei in *Cu*Mn(1 at. %) is about 600 G, as reported in Ref. 10. By scaling this field with the ratio of the Knight shift, we estimate the RKKY field at the muon site to be about 10 G.
[26]C. Held and M. Klein, Phys. Rev. Lett. **35**, 1783 (1975).
[27]R. W. Walstedt and L. R. Walker, Phys. Rev. B **9**, 4857 (1974).
[28]R. Kubo, Hyperfine Interact. **8**, 731 (1981).
[29]R. Kubo and T. Toyabe, in *Magnetic Resonance and Relaxation*, edited by R. Blinc (North-Holland, Amsterdam, 1967), p. 810.
[30]M. R. MacHenry, B. G. Sibernagel, and J. H. Wernick, Phys. Rev. B **5**, 2958 (1972).
[31]A. T. Fiory, Hyperfine Interact. **8**, 777 (1981).
[32]Y. J. Uemura, Solid State Commun. **36**, 369 (1980).
[33]This spectrometer was built by C. W. Clawson, K. M. Crowe, and their colleagues, and is described in detail in Ref. 20.
[34]In this context, the data analysis performed by K. Emmerich, F. N. Gygax, A. Hintermann, H. Pinkvos, A. Schenck, Ch. Schwink, and W. Studer [J. Magn. Magn. Mater. **31-34**, 1361 (1983)] is not appropriate. The dynamic effect of fluctuating moments is not properly taken into account in their approach.
[35]Preliminary results for a_s and λ_d in *Cu*Mn(1 at. %) were presented at the Yamada Conference for Muon Spin Rotation, Shimoda, 1983, by Y. J. Uemura, T. Yamazaki, D. R. Harshman, M. Senba, J. H. Brewer, E. Ansaldo, and R. Keitel [Hyperfine Interact. **17-19**, 453 (1984)].
[36]The values of a_s in *Au*Fe(1 at. %) was first presented at International Conference on Magnetism ICM'82, Kyoto, 1982 by Y. J. Uemura and T. Yamazaki [J. Magn. Magn. Mater. **31-34**, 1359 (1983)].
[37]R. H. Heffner, M. Leon, M. E. Schillaci, D. E. MacLaughlin, and S. A. Dodds, J. Appl. Phys. **53**, 2174 (1983). The relaxation function used to deduce the values of a_s in *Ag*Mn in this reference is not rigorously correct, since the effect of a fluctuating dynamic component is not included in the rate of initial quick damping of $G_z(t)$.
[38]C. E. Violet and R. J. Borg, Phys. Rev. **149**, 540 (1965).
[39]S. Chikazawa, S. Taniguchi, H. Matsuyama, and Y. Miyako, J. Magn. Magn. Mater. **31-34**, 1355 (1983), and unpublished.
[40]Y. J. Uemura, Ph.D. thesis, University of Tokyo, 1982.
[41]The basic points for the comparison of μSR with χ_{ac} and NSE was presented by Y. J. Uemura at the Yamada Conference on Muon Spin Rotation, Shimoda, 1983 [Hyperfine Interact. **17-19**, 447 (1984)].
[42]L. R. Walker and R. E. Walstedt, J. Magn. Magn. Mater. **31-34**, 1289 (1983), and references therein.
[43]F. Mezei and A. P. Murani, J. Magn. Magn. Mater. **14**, 211 (1979).
[44]A. P. Murani, F. Mezei, and J. L. Tholence, Physica **108B**, 1283 (1981); A. P. Murani, J. Magn. Magn. Mater. **22**, 271 (1981).
[45]J. L. Tholence, Solid State Commun. **35**, 113 (1980), and private communication.
[46]F. Mezei, J. Magn. Magn. Mater. **31-34**, 1327 (1983).
[47]Y. J. Uemura and S. M. Shapiro (unpublished).
[48]See A. P. Murani (Ref. 44) for the neutron time-of-flight results in *Cu*Mn(3 at. %).
[49]S. Kirkpatrick and D. Sherrington, Phys. Rev. B **17**, 4384 (1978).
[50]N. Ahmed and T. J. Hicks, Solid State Commun. **15**, 415 (1974); J. R. Davis and T. J. Hicks, J. Phys. F **9**, 753 (1979).
[51]J. W. Cable, S. A. Werner, G. P. Fincher, and N. Wakabayashi, Phys. Rev. Lett. **49**, 829 (1982).
[52]J. Souletie and R. Tournier, J. Low Temp. Phys. **1**, 95 (1969).
[53]D. E. MacLaughlin, Hyperfine Interact. **8**, 749 (1981).
[54]H. Sompolinsky and A. Zippelius, Phys. Rev. B **25**, 6860 (1982).
[55]K. L. Nagi and C. T. White, Phys. Rev. B **20**, 2475 (1979); A. S. Arrott and B. Heinrich, J. Magn. Magn. Mater. **31-34**, 1084 (1983).
[56]R. V. Chamberlin, G. Mozurkeiwich, and R. Orbach, Phys. Rev. Lett. **52**, 867 (1984).
[57]Data analyses based on the approach similar to the present article were employed in Refs. 13–16, 37 and 58.
[58]D. E. MacLaughlin, L. C. Gupta, D. W. Cooke, R. H. Heffner, M. Leon, and M. Schillaci, Phys. Rev. Lett. **51**, 927 (1983); R. H. Heffner, M. Leon and D. E. MacLaughlin, [Hyperfine Interact. **17-19**, 457 (1984)]; R. H. Heffner and D. E. MacLaughlin, Phys. Rev. B **29**, 6048 (1984).
[59]Some data of neutron-spin echo in *Cu*Mn(1.0 at. %) were reported in Ref. 44, but only for two temperature points.